THE STAR FORMATION HISTORY OF THE STARBURST REGION NGC 2363 AND ITS SURROUNDINGS [1,2]

LAURENT DRISSEN, JEAN-RENÉ ROY, CARMELLE ROBERT and DANIEL DEVOST[3]
Département de Physique, Université Laval and Observatoire du mont Mégantic
Québec, QC, G1K 7P4, Canada
Electronic mail: ldrissen, jrroy, carobert, ddevost@phy.ulaval.ca

RENÉ DOYON
Département de Physique, Université de Montral and Observatoire du mont Mégantic
Montréal, QC, H3C 3J7, Canada
doyon@astro.umontreal.ca

ABSTRACT

We present *Hubble Space Telescope* optical images and UV spectra, as well as ground-based near-infrared images of the high surface brightness giant H II region NGC 2363 (NGC 2366-I) and its surroundings. The massive star content of the southern end of the dwarf irregular galaxy NGC 2366 is investigated, with an emphasis on Wolf-Rayet and red supergiant stars, and we attempt the reconstruction of the time sequence of the most recent episode of massive star formation at the southwestern tip of the galaxy. The ages of the clusters are respectively 10 Myr for NGC 2366-II, 2.5-5 Myr for NGC 2363-B and less than 1 Myr for NGC 2363-A. In particular, we show that the most massive super cluster A of NGC 2363 is still embedded in dust; from the photoevaporative erosion or "cleaning" time scale of the associated cloud, we infer its age to be $\sim 10^6$ yr or less. We conclude that the star-forming complex NGC 2366-I and II is a good example of a multiple stage starburst with a characteristic age decreasing from 10 Myr to less than 1 Myr over a linear scale of 400 pc. The age sequence of the stars and the gas kinematics suggest that these powerful star formation episodes are being triggered by a small passing-by satellite.

Subject headings: ISM: individual (NGC 2363) — galaxies: individual (NGC 2366) — stars: emission line, Be — stars: evolution

1. INTRODUCTION

One of the most powerful local starburst events is taking place in the nearby magellanic galaxy NGC 2366. This activity is betrayed by three giant H II regions, one of them having its own NGC number (NGC 2363 = Mkn 71) and being the highest surface brightness H II region in the sky. By its stellar content and star formation rate, NGC 2363 competes with 30 Doradus in the Large Magellanic Cloud (Kennicutt 1984).

---

[1]Based on observations with the NASA/ESA Hubble Space Telescope, obtained at the Space Telescope Science Institute, which is operated by AURA, Inc., under NASA contract NAS5-26555

[2]Based on observations obtained at the Canada-France-Hawaii Telescope, which is operated by the National Research Council of Canada, the Centre National de la Recherche Scientifique de France, and the University of Hawaii

[3]Also at Space Telescope Science Institute, 3700 San Martin drive, Baltimore, MD, 21218

Therefore NGC 2363 has been the target of multiple studies, and many of its properties in the ultraviolet and optical domains are well known; its oxygen abundance is about 1/10 solar (Peimbert, Peña, & Torres-Peimbert 1986; Gonzlez-Delgado *et al.* 1994; although see Luridiana 1998 for a different interpretation of the data leading to a higher abundance), where 12 + log $O/H_{\odot}$ = 8.87 (Grevesse, Noels, & Sauval 1996). It has a well determined carbon abundance (Garnett *et al.* 1995). Its shows unusual kinematic features: an expanding supershell (Roy *et al.* 1991) and hypersonic gas (Roy *et al.* 1992; Gonzlez-Delgado *et al.* 1994). Only a few Wolf-Rayet stars are present; they are associated with the eastern cluster of NGC 2363 that we will also call knot B (Drissen, Roy, & Moffat 1993, hereafter DRM). Surprisingly, as we will show, we do not see the stars of the main ionizing cluster, called knot A, in NGC 2363. A rare Luminous Blue Variable, located 5″ east of this cluster, has been undergoing a spectacular eruption since about 1994 (Drissen, Roy, & Robert 1997); this star, NGC 2363-V1, is presently the brightest optical source in the galaxy. We are monitoring it spectroscopically with the Hubble Space Telescope (HST program 7391). The rich and complex system of ionized gas filaments and shells in the southwestern of NGC 2366 has been investigated by Hunter & Gallagher (1997) and Martin (1998). Martin has derived ages for the largest supershells (τ = 0.6 R/v) as 7.9 Myr for the supershell east of NGC 2366-I and II and 5.7 Myr for the shell north of NGC 2366-I (= NGC 2363). Hunter & Gallagher have infered older ages.

In this paper, we analyse optical images and ultraviolet spectra obtained with the Hubble Space Telescope (HST), as well as near infrared CFHT images, to understand the intense star formation in the three main H II regions of NGC 2366, identified as NGC 2366 I (= NGC 2363), II and III (Figures 1 and 2). In particular, we will demonstrate that the southwestern tip of NGC 2366 is undergoing a passing wave of star formation, moving from east to west, and that the most recent burst is so young that its stellar supercluster is still dust embedded; its stars are not yet seen in the ultraviolet or optical domains. We will explore the starbursting process by dating the propagating star formation process in the galaxy, and will discuss the possibility of a trigger by a small interacting satellite.

2. OBSERVATIONS

2.1. Imagery

Most of the images of NGC 2366 used in this work were obtained in 1996 January with the WFPC2 camera aboard the *Hubble Space Telescope*; the giant H II region NGC 2363 is located at the center of the high resolution PC1 CCD. At the adopted distance of 3.44 Mpc (Tolstoy *et al.* 1995), the scale is ∼17 pc/arcsec (i.e. 0.8 pc/pixel on the PC1). The broadband F439W (∼ Johnson B; 3 exposures of 900 s) and F547M (∼ Stromgren y; 2 × 800 s) filters were used. The F547M filter was prefered to the wider, more standard F555W filter, because it excludes the strong [O III] λλ4959-5007 nebular lines. However, because of the high surface brightness of the NGC 2363 nebula, dust scattered stellar light and diffuse nebular *continuum* contaminates both F439W and F547M images. Narrowband images of the same regions were obtained with the following filters: F656N (Hα; 2 × 500 s), to study the distribution of the ionized gas and F469N (He II λ4686; 5 × 2000 s) to detect Wolf-Rayet stars and a possible diffuse nebular component. During our monitoring of NGC 2363-V1, we obtained two series of short exposures covering NGC 2363 with filters F170W, F336W, F547M and F108M in 1998 March and December. Only the brightest stars are seen in these images, but they were used to determine the flux of clusters A and B. We have used DAOPHOT (Stetson 1987) to derive instrumental magnitudes and colors of the stars, and the prescription of Whitmore (1995) and Holtzmann *et al.* (1994) to transform these into the standard photometric system.

In addition to the HST observations, a 10 minute $H\alpha$ image of NGC 2366 was secured with the Loral $2K \times 2K$ CCD of the Canada-France-Hawaii telescope (CFHT) in 1996 February. The $H\alpha$ image, shown in Figure 1, outlines the location of the WFPC2 field. The WFPC2 frame, a composite of the F547M, F439W and F656N images, is displayed in Figure 2. We also obtained JHK images with the MONICA infrared camera (Nadeau *et al.* 1994) attached at the f/8 focus of the CFHT in 1997 January. The K band image is displayed in the bottom part of Figure 3 with the high resolution PC1 image (top part). Basic data reduction was performed for the infrared images using software developed by the Montréal group (D. Nadeau). The images were flux calibrated using the IR UKIRT standard stars FS2, FS21, and FS25. The uncertainties in the JHK magnitudes are ~ 0.15 mag. For a detailed description of the infrared reduction steps and calibration, see Devost (1999).

2.2. Spectroscopy

HST *Faint Object Spectrograph* spectra of NGC 2363's knots A and B were gathered in 1996 December, with the G130H grating (covering the 1140 to 1606 Å range with a resolution of 1 Å per diode) and the 0.86″-wide circular aperture. The observations were obtained as follows. The January 1996 WFPC2 images were used to identify a bright (V=17) isolated star 80″ north of NGC 2363; its position and offsets from the two targets were then measured with the IRAF/STSDAS task METRIC. This star was centered in the FOS aperture with a series of ACQ/BIN and ACQ/PEAK acquisition sequences, leading to a pointing accuracy of about 0.04 arcsecond (Keyes *et al.* 1995). The telescope was then slewed to cluster A and the observation took place. The telescope was slewed back to the offset star, re-centered in the aperture before coming back to cluster B. The total integration times were 6150 s for cluster A and 9730 s for cluster B.

Moreover, we obtained a series of HST/STIS long slit spectrograms of NGC 2363-V1 in 1997 November with the G140L and G230L gratings in order to study the physical parameters of this erupting LBV. The spectra of V1 will be discussed elsewhere (Drissen *et al.* 1999a), but two bright stellar objects (stars or unresolved stellar aggregates) within NGC 2363-B fell by chance into the slit and provide us with valuable information about the stellar content of this cluster (section 4.3).

3. THE STARBURST COMPLEX NGC 2366-I AND II: AN OVERVIEW

The massive star population of NGC 2366, with the notable exception of the core of NGC 2363, is generally well resolved into individual stars in our images (Figure 2). The F547M image reaches V$\sim$ 25.5; this corresponds to $M_v \sim -2.5$, or spectral type B2 ($M \sim 10 M_\odot$) on the main sequence. On a deep Hα image (Figure 1), NGC 2366-I and II appear like a single, high surface brightness ionized gas complex. But the high resolution continuum images reveal that they are two distinct entities with their own star-formation history. NGC 2366-III, discussed in more detail in section 5, appears like a group of loose OB associations without a well-defined core. The WFPC2 (F547M) and MONICA (K-band) images of NGC 2366-I and II are displayed in Figure 3. Red supergiant stars identified in the color-magnitude diagrams (with $B-V \geq 1.0$ and $M_V \leq -5.0$ in Figure 4) are circled. We also note the presence of a slightly resolved source, at the eastern edge of NGC 2363, which is bright in the K image, but barely detected in the J and H images. The near-IR colors of this object are those of hot ($\sim$ 500 K) dust.

The spatial distribution of the red supergiants is reflected in the two color-magnitude diagrams: the difference between NGC 2363 and NGC 2366-II is striking. Only three red supergiants are seen in the CMD

of NGC 2363; in fact, these stars are located outside the main body of the H II region and may not be physically related to it. In contrast, more than two dozen red supergiants are seen within the boundaries of NGC 2366-II. The surface density of these stars is much higher in NGC 2363-II than in the rest of the galaxy, attesting to their association with the H II region. Their red supergiant nature is also confirmed by the MONICA J, H and K images and the near-infrared two-color diagram (Figure 5); this diagram will be discussed in more details below. The presence of such a large number of red supergiant stars in a giant H II region is uncommon and suggests that the main burst of star formation in NGC 2366-II occured some 7 to 10 Myrs ago (Mayya 1997); this is consistent with the age of supershell A (Martin 1998). On the other hand, many bright, blue stars are seen in the western part of NGC 2366-II, close to the bright Hα ridge visible in Figure 2. These are certainly younger than most red supergiants seen in the eastern section of the cluster; their presence suggests that the star formation process in NGC 2366-II did not occur in a single, instantaneous burst. We are probably seeing here a slightly more evolved version of the two-stage starburst NGC 2363 itself (see next section).

4. NGC 2363

In ground-based continuum images, NGC 2363 presents a double morphology with two intensity maxima that we identified (DRM) as western knot (A) and eastern knot (B). The new HST images now resolve B into an elongated, bright (V$\sim$18), slightly resolved core surrounded by many dozens blue stars (Figure 6). From now on we shall refer to the OB association, within the boundaries of the expanding cavity, as "cluster B", and the compact object at its core as "knot B". The western half of NGC 2363 contains few visible stars and has a very high Hα surface brightness. What appears at its core, knot A, remains unresolved into stars; we will show below that because of dust we do not see stellar light directly. Actually, the different nature of knots A and B is also made clear in the near-infrared two-color diagram (Figure 5): we see that knot B has near-IR colors of hot, blue stars, while the colors of knot A are very similar to those of a pure H II region (see Figure 5 in Doyon *et al.* 1995).

4.1. The Population of Wolf-Rayet Stars

Wolf-Rayet stars in cluster B of NGC 2363 were first detected by DRM via narrow-band filter imagery. The excess of light at λ4686 was then attributed to the presence of about 5 WR stars, although a contribution from a *nebular* component could not be excluded and was indeed suggested by the images. Long-slit spectroscopy (González-Delgado *et al.* 1994) confirmed both the WR and nebular signatures: apart from a strong, *narrow* He II λ 4686 emission line of nebular origin, broad bumps at 4660 Å and 5800 Å, typical of WR stars, are detected. The ratio of the 4650 and 5800 Å bumps indicates that an early-type WC star dominates the WR population in cluster B.

The WFPC2 images provide a clearer picture. In order to identify the WR stars, we subtracted the continuum image (a weighted average of the F547M and F439W images) from the F469N image (see Drissen *et al.* 1999b for more details); the result is shown in Figure 7. The quality of the image subtraction can be judged by the very low residuals at the position of knot A. The largest *absolute* residuals on the net image are at the position of V1, which is by far the brightest star in the field; they amount to $\pm$ 5% of the peak value of the stellar PSF in the continuum image. The total net counts within the PSF of V1 in the net image is, within 1 σ, identical to the total counts in a nearby region of the sky.

Three stars in cluster B clearly have an excess of light at 4686 Å; a fourth one is detected 8.6″ (140 pc) north of the cluster. WR1 has a continuum magnitude ($M_v \sim -5.5$) typical of Galactic WR stars. The λ 4686 excess detected at the northwestern tip of the elongated core of cluster B (WR2) could be the result of an imperfect image subtraction due to the complex distribution of light in this region, but all our attempts to make it disappear by shifting the images around before subtraction failed, and we are confident that it is real and betrays the presence of a WR star. The star with the strongest λ 4686 excess, WR3, is very likely the WC star which dominates the global WR spectrum of the region. With $M_v \sim -7$, this star appears much brighter than any known WC star, but it is very likely that we are in fact observing an unresolved stellar aggregate which includes one WC star. Finally, the isolated WR4 has a weak, but significant excess, suggesting that it might be a narrow-lined WNL star. We note that a weak residual also appears in the net 4686 image of DRM (see their Figure 3) at the same position as WR4, but was not discussed in their paper. WR4 is located 150 pc (projected distance) from the center of cluster B and its association with the later is not clear.

No WR candidate, nor significant diffuse He II λ4686 emission are detected near cluster A, nor in NGC 2366-II. It is worth emphasizing that no other WR candidate has been detected anywhere else in the galaxy despite a very careful search, using both the subtraction technique and by blinking the continuum and "on-line" F469N frames. Using the same techniques and similar exposure times, we detected a large number of WR candidates in NGC 2403 (about 40 per WFPC2 field), a spiral galaxy at the same distance as NGC 2366 (see Drissen *et al.* 1999b, where incompleteness is also discussed in detail).

The small number of WR stars in and around NGC 2363 is very surprising at first sight. Giant H II regions with similar Hα luminosities such as 30 Dorarus in the LMC or NGC 2403-I and II, host between one and two dozen WR stars each. NGC 604 and NGC 595 in M33 also have a substantial WR population (Drissen, Moffat & Shara 1993). This paucity of WR stars in NGC 2363 can be explained by two factors. The metallicity of NGC 2363 has generally been determined to be close to one tenth solar (Peimbert *et al.* 1986). At this low metallicity, very few O stars (those more massive than ~ 80 $M_\odot$) are expected to shed enough mass via their wind to reach the WR phase (Schaerer & Vacca 1998). But Luridiana (1998) suggests that the metallicity of this region has been underestimated, and that a value of $Z = 0.25 Z_\odot$ would give a better fit to the observed line ratios. The higher value is also consistent with the mean abundance level established by Roy *et al.* (1996) for the other regions of NGC 2366. If this value is adopted, then the number of WR stars ought to be comparable to that of 30 Dor. Nevertheless, we think that the age spread within NGC 2363 provides a better explanation: as we will explain below, cluster A provides the bulk of the ionizing flux for the nebula, but we do not see a signature of WR stars because (a) it is much too young to harbor a sizeable WR population and (b) its stars are still hidden in dust.

4.2. The He II Nebular Excess and its origin

Ground-based narrow-band imagery suggest the presence of a spatially extended nebular He IIλ 4686 emission ($l \sim 4''$) in NGC 2363; this has been confirmed spectroscopically (see references above). In order to check if this diffuse component was also detected in the WFPC2 images, we first subtracted the point sources (i.e. WR candidates) from the net λ 4686 image shown in Figure 7, using DAOPHOT's substar task. The resulting image was convolved with a gaussian profile of 1.5 pixel radius to increase the signal-to-noise ratio. Figure 8 presents the monochromatic Hα image of NGC 2363, with the contours of nebular He IIλ 4686 emission superposed. The total flux from this diffuse component is $F_{neb}^{4686} = 2.5 \times 10^{-15} erg\ cm^2\ s^{-1}$, a value which is compatible with the spectroscopic data of Gonzlez-Delgado *et al.* (1994). The faint extended

zone of nebular He IIλ4686 emission corresponds to an obvious cavity in overall emission and its orientation is the same as that of the "chimney" discovered by Roy *et al.* (1991). Garnett *et al.* (1991) have reviewed the possible ionization mechanisms for nebular He II emission. They are:

1. *Hot stellar ionizing continua.*– Classical nebulae ionized by O stars having $T_{eff} \leq 55{,}000$K do not produce strong He^{++}. However models for massive stars with mass loss (Maeder & Meynet 1987) predict evolution blueward to $T_{eff} \geq 70{,}000$ K. Pakkull (1991) suggest that very early WN-type stars do have T_{eff} high enough to excite He II emission. WO stars could have very high temperatures and be capable of producing the He^{++} zone, but the spectrum of cluster B (Gonzlez-Delgado *et al.* 1994) does not show the broad OVI λ3811,34 lines characteristic of WO stars. Schaerer & Vacca (1998) show that nebular He II emission should be associated with WC/WO stars and hot WN stars evolving to become WC/WO stars. WO stars would show very strong and broad P Cygni profiles in the O VI lines. WNE would also show high excitation features such as P V and S VI but no O VI lines.

2. *Shock excitation.*– Shocks can produce relatively strong He II emission when shock velocities are $\sim$ 120 km/s or higher (Binette, Dopita & Tuohy 1985; Sutherland, Bicknell, & Dopita 1993). However ground-based spectra do not reveal evidence for shocks, and the mean velocity of the expanding supershell revealed by Roy *et al.* (1991) is about 45 km/s.

3. *X-rays.* – X-ray sources could have enough flux extending into the extreme UV to produce He^{++} nebulae (Pakull & Angebault 1986). No X-ray source is known to exist in NGC 2363; but it could always be hypothesized that the He^{++} zone is a fossil from an X-ray source which switched off within the past century (Garnett *et al.* 1991).

We have shown that 3 WR stars are present at the core of cluster B. None of them is a WO, but the global spectrum being one of a hot WC4 star, we suspect that they supply a good fraction of the hard UV-flux which is the source of the nebular He II emission in NGC 2363. Observations with FUSE could help to identify these stars.

4.3. Selected Stars

NGC 2363-V1 is, since early 1995, the most luminous star in its galaxy. Once too faint to be detected in ground-based images, it is now $M_v \sim -10.5$. Analysis of its light curve and spectrum shows that it is a Luminous Blue Variable experiencing a major eruption, probably similar to that of η Carina in the middle of the 19^{th} century (Drissen *et al.* 1999a). The luminosity of V1 prior to its current eruption was much lower than that of η Car, so it is likely to be older (age $\sim$ 4 to 5 Myrs) and less massive than its Galactic counterpart.

By chance, the long slit we used to obtain the STIS spectrum of V1 intercepted the light from two stellar objects (identified as stars 1 and 2 in Figures 5 and 6). While the image of star 1 appears unresolved, star 2 is obviously multiple. Both objects are too bright to be single stars, and their spectra are likely to be composite. These are shown in Figure 9, along with those of stars having similar spectral morphology in the Small Magellanic Cloud. Actually, these SMC templates are averages of a few stars having the corresponding spectral type, a part of the spectral library built by C. Robert. Evolutionary synthesis models predict an age of 3 to 5 Myr for a cluster with an O5 II star spectrum and 4.5 to 7 Myr for a cluster with an O9 III star spectrum.

We also note the presence of two blue stars surrounded by H II shells, located about 100 pc south of

knot A (see Figure 6). The shells have a diameter (2 and 6 pc, respectively) similar to those of Galactic LBVs. These objects warrant further spectroscopic investigation.

4.4. The FOS Ultraviolet Spectra of Knots A and B

The FOS UV spectra of knots A and B are presented in Figure 10. To increase the signal-to-noise ratio, the data were smoothed using a boxcar filter over four pixels (the original spectral resolution is maintained as the spectra were oversampled by quarter-diode subpixel steps). The FWHM of simple interstellar lines (SiI 1254, SiII+SiII 1260, OI+SiII 1303, and SiII 1527) and of the Lyα geocoronal line reveal an average spectral resolution $\lesssim 2$ Å, consistent with the expected resolution of the G130H grating. In order to properly interpret the spectral synthesis, the spectra have been shifted to position the interstellar lines at their rest frame wavelength. Shifts of -190 and -150 km s^{-1} were applied to the spectra of knots A and B, respectively. Given the known systemic velocity of NGC 2363, +110 ($\pm$10) km s^{-1} (Izotov, Thuan & Lipovetsky 1997), the remaining velocity (i.e. 80 and 40 km s^{-1} for A and B, respectively) is mainly due to the uncertainty in measuring the zero-point of the instrument wavelength scale, which is typically of the order of 130 km s^{-1}.

The spectrum of knot B reveals strong P Cygni profiles at 1550 Å (the CIV doublet at 1548.2 and 1550.8 Å) and at 1240 Å (the NV doublet at 1238.8 and 1242.8 Å). These are typical signatures of fast and dense stellar winds from massive stars (see the UV atlas of O stars by Walborn, Nichols-Bohlin & Panek 1985). Many UV resonance lines, like CIV and NV, are also formed in stellar photospheres and the interstellar medium, in which case they appear as absorption lines only without an emission component. A narrow interstellar contribution to CIV is indeed seen superposed on the wind profile of knot B.

Another important clue to the stellar content of knot B is the fact that the SiIV 1400 line (at 1393.8 and 1402.8 Å), also a resonance doublet, does not show a wind P Cygni profile in this spectrogram. Because the Si^{+3} ion has a smaller opacity than C^{+3}, SiIV, unlike CIV, develops a P Cygni profile only in the denser winds of giant and supergiant stars, and remains a photospheric absorption line in main sequence hot stars. The weak absorption line at 1371 Å (OV; see Walborn *et al.* 1985) is typical of mid-temperature main sequence to giant O stars; this line is seen as a broad P Cygni line in O3 stars or O supergiants and disappears in late O and B stars. If late B stars were the main contributors to the UV lines of knot B, their photospheric absorption lines, which are broader than their counterparts in O stars or the interstellar medium, would show up in the spectrum; this is not the case.

This first qualitative look at the spectrum of knot B already tells us that this stellar population must be dominated by massive, young O stars at a time before most of them have evolved into giants or supergiants. Knot B must therefore be young (i.e. a few Myr only), as we will determine more quantitatively from the UV line synthesis below.

The spectrum of knot A is strikingly different from that of knot B: it is much flatter and does not harbor P Cygni wind profiles. There is no sign of stellar wind signatures at CIV 1550, NV 1240 nor SiIV 1400, nor indications of cooler B stars with broad photospheric lines. The CIV 1550 feature in knot A is actually a strong narrow nebular emission, consistent with the very high nebular surface density seen in the Hα image. An HST/FOS spectrum of knot A covering the wavelength range from 1600 to 2300 Å (Garnett *et al.* 1995) also shows many nebular emission lines of OIII] 1666, SiIII] 1883, 1892, and CIII] 1909. The slope of the continuum over the whole region covered by the FOS is consistent with a purely nebular continuum and stellar light scattered by dust. We do not associate the weak continuum depression blueward of the CIV emission with a wind signature, but rather attribute it to a sequence of many absorption lines (of SiII and

possibly FeIV) of interstellar origin. We therefore come to the surprising, but interesting, conclusion that *the massive young stars responsible for the photoionization of knot A and its surrounding are not detected in the ultraviolet spectrum and are therefore completely hidden from view at this wavelength.*

4.5. Spectral Synthesis of the UV spectrum of knot B

We perform the UV spectral synthesis of knot B using the code of Dionne (1999). This code is a revised version of the code of Leitherer, Robert & Drissen (1992) and a slightly different version of the Starburst99 code (Leitherer *et al.* 1999). The Dionne code is optimized for UV spectral synthesis at various metallicities (and for the treatment of massive close binaries). It contains a library of UV spectra (normalized to a continuum equal to unity) at medium-high resolution of O, B and WR stars in the solar neighbourhood and the lower metallicity environment of the Small and Large Magellanic Clouds. It uses the recent evolutionary tracks of the Geneva group (Charbonnel *et al.* 1993, Schaller *et al.* 1992, Schaerer *et al.* 1993a, b, Meynet *et al.* 1993), interpolated to the metallicity of the Magellanic Clouds. Stellar atmosphere models (Kurucz 1992 for OB stars, Schmutz, Leitherer & Gruenwald 1992 for WR stars) are used to flux-calibrate the UV library spectra. The code follows a population of stars where at each time step the stellar evolutionary tracks give, among other paramaters, the effective temperature and luminosity of each star which are used to assign a spectral type, and then a UV spectrum from the library.

At first, we synthesize the UV spectra of knot B for a stellar population at low metallicity with the evolutionary tracks at 0.1 $Z_{\odot}$ and the SMC UV library (built with HST UV spectra of O stars from the SMC and IUE spectra of WR and B stars in the solar environnement). A Salpeter type IMF is considered, i.e. a power law with an exponent $\alpha = 2.35$, with the lower mass limit $M_{low} = 1\ M_{\odot}$ and upper mass limits $M_{upp} = 30$ to 120 $M_{\odot}$. The star formation rate is either constant, i.e. new stars are created at each time step, or instantaneous, i.e. all stars are formed at an initial time.

For the instantaneous models, the best agreement between the synthesized wind lines and the observation is found for $M_{upp} = 60$ to 120 $M_{\odot}$ and the corresponding ages $\tau = 3$ to 2 Myr. With a higher upper mass limit, younger models are favored because the absorption part of the wind profiles of SiIV and CIV becomes too deep too fast. If the upper mass limits is bellow 60 $M_{\odot}$, the models do not predict enough wind signatures in CIV. For older ages, the wind contribution predicted for SiIV is too strong. These wind effects disappear with the death of the massive stars. Around 7 Myr, SiIV becomes a broad absorption, CIV is a weak P Cygni profile (formed in B supergiants), NV is absent and photospheric lines of SiIII around 1300 Å are predicted. NV is not very well reproduced with the best models (i.e. the predicted strength of the P Cygni emssion is not large enough at young ages), but this line has a lower weight due to its strong blending with Lyα which is not well reproduced by the library spectra.

In the case of the continuous models, the age is slightly stretched by 0.5-1 Myr and the upper mass limit lower value increased to 80 $M_{\odot}$. Indeed, since the best fits are found for a young age, the new stars added in the continuous case are not numerous enough yet to dilute the wind signatures. Other models have been considered with various IMF parameters. Good fits are found for a lower IMF exponent or an increased lower mass value (i.e. when the massive stars are more numerous relative to the low mass stars). But this has little effect on the age and the upper mass cutoff. If the metallicity is increased (e.g. $Z = 0.25\ Z_{\odot}$ with the LMC UV library), the strength of the wind profiles are strong at an earlier age and for a lower upper mass limit, but then it becomes impossible to reproduce simultaneouly the SiIV and CIV lines.

Figure 11 shows a superposition of the observed spectrum of knot B with synthetic spectra at different

ages for an instantaneous model with $\alpha = 2.35$ and $M_{upp} = 80\ M_\odot$. The observed spectrum is dereddened so the UV continuum slope reproduces the theoretical slope for a young burst at low metallicity (i.e. with the UV flux $F \propto \lambda^\beta$, $\beta = -2.7$; Leitherer *et al.* 1999). Using the SMC extinction law of Prvot *et al.* (1984), a galactic contribution $E(B-V)_{Gal} = 0.04$, we find the small internal extinction $E(B-V)_{Internal} = 0.018$. The best fit to the data, corresponding to an age of 2.5 Myr, is shown superposed on the observed spectrum in Figure 11. As discussed already, younger models do not show the strong wind line of CIV. Older models give, at first, too much wind signatures in SiIV. With the death of the most massive stars, the wind profiles disappear and broad B stars absorptions appear. As we can see in Figure 11, none of the best fits are perfect in the center of CIV. The residual between the models and the observation shows a large emission component of unknown origin with a velocity width (FWZI) of ~ 2000 km s^{-1}, centered on CIV.

Assuming a distance of 3.44 Mpc, the synthesis code allows to estimate, based on the best line models, that about 800 B stars and 40 O stars are present in knot B. Three WR stars are seen from images in narrow bands. However, no WR stars are predicted by the population synthesis models that best match the UV spectra: the first WR star to appear at a metallicity of 0.1 $Z_\odot$, when stars as massive as 120 $M_\odot$ are present, is at around 2.8 Myr. On the one hand, the evolutionary tracks for the massive stars we use are still in developement. For example, rotation effects are being included which will possibly modify the time at which the first WR star will appear (Maeder 1999). Furthermore, as we are studying a small population, fluctuation in the IMF must be expected.

We now compare the light and energy output predicted by the population synthesis model (age=2.5 Myr, Salpeter IMF, Z = 0.1 $Z_\odot$) that best reproduces the UV spectra of knot B with the observations.

- *V magnitude* - The predicted unreddened flux at 5500 Å is 3×10^{-16} erg s^{-1} Å^{-1} cm^{-2}. From the WFPC2 images, we measure a total magnitude $V = 18.5$ within a radius of $0.43''$ (to match the FOS aperture) centered on knot B. This corresponds to 2.2×10^{-16} erg s^{-1} Å^{-1} cm^{-2} if we adopt $A_v = 0.4$, in relatively good agreement with the population synthesis models.

- *Ionizing photons* - The total number of Lyman continuum photons produced by massive stars in knot B is $LogN_{Lyc} = 50.78$, that is about 6% of the number required to ionize the entire nebula. This suggests that the most important source of ionization in NGC 2363 comes from knot A.

- *Kinetic energy* - Finally, the total energy returned to the ISM since the starburst 2.5 Myrs ago via stellar winds is of the order of 5×10^{50} erg (we note here that this energy is a factor of 10 smaller than the same stars would generate in a solar metallicity environment; see Leitherer *et al.* 1999). This is 2 orders of magnitude smaller than the kinetic energy in the expanding bubble discovered by Roy *et al.* (1991, 1992). Since the bubble cannot have been blown by the winds of massive stars in the core of cluster B, we conclude that the energy released by the winds of massive stars and especially supernova explosions within the bubble but outside the knot B are responsible for the bubble expansion. As we showed in section 4.3, there are hints that the stellar population surrounding knot B is a bit older than the core itself, an age segregation that we also observe in the super star clusters of NGC 2403 (Drissen *et al.* 1999b).

4.6. Dust Embedded Super Stellar Cluster of Massive Stars at Knot A

All the information we have gathered so far, namely the existence of 3 WR stars, the spectral features of stars 1 and 2 and the core, the absence of red supergiants, and the kinematical age of the bubble, indicate

that cluster B is 2.5 to 5 Myr old, with a real age spread between the core and the periphery. We now show that cluster A is even younger.

The western half of NGC 2363, surrounding knot A, has a high Hα luminosity and exceptional surface brightness. It must therefore be ionized by a rich young cluster of massive stars characterized by a UV continuum sharply rising towards shorter wavelengths and full of P Cygni profiles. This is obviously not what we see: the absence of stellar features in the flat UV spectrum of NGC 2363-A strongly suggest that the super star cluster responsible for most of the ionization of NGC 2363 is completely shrouded in dust. Despite the low apparent extinction derived from the Balmer decrement (c(Hβ) $\sim$0.2), the presence of dust in the nebula is obvious even in the optical domain. NGC 2363 is a very high surface brightness object and its electron temperature at T = 15 000 K is unusually high (Kennicutt, Balick, & Heckman 1980; Peimbert *et al.* 1986; Gonzlez-Delgado *et al.* 1994). Thus we can expect the nebular continuum to be relatively strong, especially in the ultraviolet where the contribution of the two-photon continuum becomes important. Dust particles scatter continuous radiation of the stars immersed in the H II region, resulting in an observable diffuse continuum (Osterbrock 1989). The main contributions to the nebular continuum in the F547M band are the hydrogen recombination continuum, the He+ recombination continuum (about 1/10 of the hydrogen one) and the 2-photon continuum; the fraction of He++ is only 0.003 of H+ (Gonzlez-Delgado et al. 1994). We make the assumption that the ratio of these continua to Hα is about the same in the Hα and F547M filter bandpasses. This is justified by the fact that the sum the H, He recombination continua and of the two-photon at 15 000 K are roughly constant between the two wavelengths (Aller 1984). The nebular continuum can then be roughly approximated by scaling the Hα image. The F547M filter should be free of all major nebular line emission. Therefore, we used this image to subtract a scaled Hα image obtained with the F656N filter (after removing the stellar profiles in both the F547M and F656N HST images using the standard techniques of the DAOPHOT package in IRAF). The remaining diffuse emission, in particular in and around knot A, is most likely due to stellar light scattered by dust; the result is shown in Figure 12. If on the larger scale, the nebular continuum probably dominates, in the brightest regions of knot A the dust scattered continuum may be up to four times stronger than the nebular continuum.

Let us now use another important piece of information: NGC 2363 shows as a point source in the IRAS Point Source Catalog with $S_{12\mu m} < 0.25$ Jy, $S_{25\mu m} = 0.7235$ Jy, $S_{60\mu m} = 3.303$ and $S_{100\mu m} = 4.578$ Jy. The flux value at 12.5μm is an upper limit. Although the IRAS spatial resolution is crude, we will show that knot A is probably the point source.

Dust embedded massive stars have remarkably similar far-infrared (FIR) flux density distributions independent of distances (Wood and Churchwell 1989a,b). On color diagrams Log [$S_{100\mu m}/S_{60\mu m}$] vs Log [$S_{25\mu m}/S_{12\mu m}$] and Log [$S_{60\mu m}/S_{12\mu m}$] vs Log [$S_{25\mu m}/S_{12\mu m}$], the FIR colors of NGC 2363 are very close to the locus of FIR colors of ultracompact H II regions (Wood & Churchwell 1989a). Since the measurement at 12μm is an upper limit, then the colors are pushed well into the regime of ultracompact H II regions. Observations of dust in galactic compact H II regions imply visual extinctions between 25 and 1250 mag (Chini *et al.* 1986 a,b).

Figure 13 presents the spectral energy distribution (SED) of the core of cluster B and of knot A, from the FOS spectra, WFPC2 and MONICA images (all within an aperture of 0.86″ to match the FOS aperture), and the IRAS data. We assume here that most of the FIR flux of NGC 2363 originates from knot A, which is a reasonable assumption given the arguments presented above. The SED of cluster B is very well fitted by an instantaneous starburst model of age 3 Myr, but the SED of knot A is very different. The flat UV to optical distribution and the huge FIR excess are in fact reminiscent of the SED of dust-embedded starburst galaxies (Silva *et al.* 1998), although the starburst in NGC 2363 is much younger that those in the galaxy

sample of these authors.

We have therefore strong evidence that the region is shrouded by dust: super cluster A is in the ultracompact H II region stage, that is that the newly formed stars are still embedded in their natal molecular clouds (Churchwell 1991). The far-infrared flux can then be used to infer the star formation rate and the dust content of the region. Following Devereux & Young (1990a)

$$L(40-120\mu\mathrm{m}) = 3.65\times10^{5}\ (2.58S_{60\mu\mathrm{m}} + S_{100\mu\mathrm{m}})\ D^{2}\ [L_{\odot}], \tag{1}$$

where $S_{60\mu\mathrm{m}}$ and $S_{100\mu\mathrm{m}}$ are the IRAS 60 and 100 μm flux densities in units of Jy, and D is the distance of the object in Mpc. For NGC 2363, L(40 − 120 μm) = 5.7 $\times10^{7}$ L$_{\odot}$. The star formation rates for the high-mass end are infered from the FIR luminosity (Devereux & Young 1991; Sauvage & Thuan 1992), as

$$SFR_{\mathrm{FIR}}(\geq 10M_{\odot}) = 1.4\times10^{-10}L_{\mathrm{FIR}}(L_{\odot})\ [\mathrm{M}_{\odot}\ \mathrm{yr}^{-1}], \tag{2}$$

or from the Hα luminosity (Kennicutt 1983), as

$$SFR_{H\alpha}(\geq 10M_{\odot}) = 5.45\times10^{-9}L_{H\alpha}(L_{\odot})\ [\mathrm{M}_{\odot}\ \mathrm{yr}^{-1}]. \tag{3}$$

With the appropriate values for NGC 2363, $SFR_{\mathrm{FIR}} \simeq 0.01$ M$_{\odot}$ yr^{-1}, and $SFR_{H\alpha} = 0.02$ M$_{\odot}$ yr^{-1} for high mass stars. Both rates are comparable, in agreement with the hypothesis that the high-mass stars which ionize the hydrogen gas generate the far-infrared luminosity (Devereux & Young 1990a).

The total mass of dust in NGC 2363 can also be estimated from the far-infrared luminosity, although several effects and uncertainties may affect the result (see Draine 1990). If we assume that the NGC 2363 far infrared luminosity is dominated by a single grain component and temperature, we have for dust heated by OB stars following Devereux & Young (1990b)

$$M_{d} = 4a\rho S_{100\mu\mathrm{m}}D^{2}/3Q_{100\mu\mathrm{m}}B_{100\mu\mathrm{m}}(T), \tag{4}$$

where $B_{100\mu\mathrm{m}}(T)$ is the value of the Planck function at 100μm, $S_{100\mu\mathrm{m}}$ is the 100 μm flux density, D is the distance, $Q_{100\mu\mathrm{m}}$ is the grain emissivity at 100μm, a is the grain radius, and ρ is the grain density. Using appropriate values for the grain parameters (Hildebrand 1977, Hildebrand *et al.* 1983), the above equation is simplified to

$$M_{d} = CS_{100\mu\mathrm{m}}D^{2}(e^{144/T}-1)M_{\odot}, \tag{5}$$

where D is the distance in Mpc, $S_{100\mu\mathrm{m}}$ is the 100 μm flux density in Jy and T is the dust temperature. C is a poorly known constant which depends on the grain opacity which can vary between about 1.8 and 4.58 (Eales, Wynn-Williams, & Duncan 1989). The total mass of dust derived is obviously very sensitive to the adopted temperature. Adopting $T_{d} \sim 30$ K (Churchwell, Wolfire, & Wood 1990), $C \sim 4$ and $D = 3.44$ Mpc, one finds $M_{d} \sim 2.6\times10^{4}\ M_{\odot}$ of dust. If we assume $M_{H_2} = 100\ M_{d}$ (Solomon *et al.* 1997), the mass of molecular hydrogen associated with NGC 2363 is of the order of $10^{6}\ M_{\odot}$. Although this figure appears reasonable, one must be aware of the associated uncertainties; this naive approach is likely to underestimate the total dust mass (Draine 1990).

One can use this estimate of dust-gas mass and the fact that the stars of super cluster A are not directly visible to infer some upper limit to its age by deriving its "cleaning time scale" (Blaauw 1991). We will suppose that most of the obscuring part is in the dense accretion disks out of which the individual stars formed. We will assume that the dominant extinction is due to the individual dusty disks, and that the gas and dust are being eroded by the steady replenishment of the explanding plasma by material photoevaporating from

neutral disks orbiting the massive stars. Using the integrated observed properties of NGC 2363 (Kennicutt 1984), we take the number of ionizing photons from the young massive stars as 10^{52} s^{-1} corresponding to a total mass of 50 000 M$_\odot$ in OB stars; the ionized mass of hydrogen is $\sim 10^6$ M$_\odot$. Disk photoevaporation around single young stars has been studied and modeled by Hollenbach *et al.* (1994). Using and scaling their global relations, which do not depend on the details of the accretion disk-star geometry, we can get a rough estimate of the lifetime of the dust and gas cloud wrapping super cluster A. The photoevaporative mass-loss rate in the strong wind case, which is the most appropriate case for NGC 2363-A, is given by

$$\dot{M} \simeq 6 \times 10^{-5}\ \Phi_{49}^{0.44}\ v_{w8}\ \ [M_\odot \mathrm{yr}^{-1}], \tag{6}$$

where $\Phi_{49} = \Phi_i/10^{49}$ s^{-1} is the photon rate, and v_{w8} is the stellar wind speed in units of 1000 km s^{-1}. The total effective photoevaporative rate in the surroundings of the massive stars of NGC 2363 would be of the order of $\geq 10^{-3}$ M$_\odot$ yr^{-1}. Thus 10^3-10^4 M$_\odot$ could be ablated in 1 Myr, a value consistent with the 1% fraction of the molecular gas residing in dense cloud cores out of which the circumstellar disks form. In a super-cluster, each star probably has its own individual accretion disk. Hollenbach et al. estimate that lifetimes of $\geq 10^5$ yr are probably achieved by 2-10 M$\odot$ disks, a range of disk masses corresponding to the critical value of ~ 0.3 M$_*$ above wich the disks are unstable. The effect of dust will lengthen these lifetimes, but in a cluster of stars-disks, the boiling away of the remnant accretion disks will be accelerated by the first stars emerge from their cocoons. Taking these various effects into consideration, a cleaning time scale of about 1 Myr is plausible. We surmise that super stellar cluster A cannot be much older than this. There are likely additional larger dust envelopes or shells somewhat decoupled from the individual stellar disks (Churchwell *et al.* 1990). These larger cocoon with lower densities than disks may rapidly develop a clumpiness which allows easy paths for photons to get through, as seen in young galactic H II regions (Cox, Deharveng, & Leene 1990).

5. NGC 2366-III

The WFPC2 image of the central part of NGC 2366-III is shown in Figure 14, and the color-magnitude diagram of the same region is displayed in Figure 15. Fifteen red supergiant stars are located within the boundaries of the H II region; their surface density there is a factor of 5 higher than in the remaining of the WF CCD, attesting to their association with NGC 2366-III. It is noticeable that most of the RSG stars are located at the periphery of the central region, where the density of ionized gas (including a possible wind-blown bubble) is higher.

6. GAS MORPHOLOGY AND KINEMATICS

Ground-based Hα imagery of NGC 2366 betrays a spectacular network of filaments and shells (Hunter & Gallagher 1997; Martin 1998). Martin (1998) has used longslit echelle spectroscopy to study these structures; she calculated various parameters (age and total kinetic energy) for the most obvious filament structures surrounding NGC 2363; she derived kinematic ages less than 10 Myr. A slightly different view is possible. Basing their arguments on models of supershell formation, Hunter & Gallagher (1997) believe that the massive stars that were the cause of the filaments cannot be those at the core of the H II regions; they suggest that these gaseous structures must be from a previous episode of star formation as old as 50 Myr. Ground-based [O III]λ5007 Fabry-Perot interferometry done at CFHT (some of the data were presented in Roy *et al.* 1991) is helpful in revealing the large scale kinematics of the ionized gas. For example, apart

from the unusual properties of the gas in NGC 2363, the [O III]λ5007 line profiles are very narrow and symmetrical in NGC 2366-II and III. While the mean heliocentric velocity of the gas is about 90-100 km/s in the "quiescent" region of NGC 2363 (we exclude the supershell and hypersonic velocity gas), and 100-110 km/s in NGC 2366-II, it is 60-70 km/s in NGC 2363-III. There is a systematic gradient between NGC 2366-I and II to III in the diffuse [O III] emission, with heliocentric velocities decreasing from 100 to 80 km/s.

The H I maps of Braun (1995) display a similar velocity range. Morever the H I column density map shows a rim of gas of lower velocity gas west of the main optical body of the galaxy, and NGC 2366-III is clearly associated with this rim. The velocity contours reveal a disturbed shape at the southwestern tip and show the same velocity difference of 30-45 km/s between NGC 2366-III and the two other large H II regions. These kinematical features suggest that NGC 2366-III may belong to a system which is kinematically disconnected from the main body of NGC 2366. We will surmise that it may be a small satellite cloud associated with NGC 2366, whose capture or interaction is responsible for triggering star formation in that region of the galaxy.

7. STARBURST TRIGGERING BY INTERACTION: A DISCUSSION

The observations presented above clearly point to a well-determined age sequence running from east to west among the star clusters. The typical age of the stellar population range from 10 Myr (NGC 2366-II) to 3-5 Myr (NGC 2363-B) to less than 1 Myr (NGC 2363-A). Although these events could be completely uncorrelated, it seems interesting to examine the possibility that a single event led to the formation of these clusters.

The relative locations and velocities of NGC 2366-III and of the associated rim of H I gas support the scenario of a satellite cloud being now in close interaction with the main body of the galaxy NGC 2366. NGC 2366-III is at a distance of 1.4 kpc, in the plane of the sky, of the mid-point between NGC 2363 and NGC 2366-II. Supposing a space velocity of 150 km/s, a realistic value for a satellite of a magellanic galaxy, NGC 2366-III was very close to the southern tip of the galaxy less than 10 Myr ago, and could have triggered the interaction which has led to the strong episodes of star formation in the southern half of NGC 2366 and in NGC 2366-III. This environment of a starbursting magellanic galaxy is not unique. Actively star forming dwarf galaxies often (in more than 50% of the cases searched) have nearby companions (Taylor 1995; Taylor *et al.* 1995). For example, Stil & Israel (1998) have recently found a low-mass H I companion to the post-starburst galaxy NGC 1569 at a projected distance of 5 kpc. The velocity difference between NGC 1569 and NGC 1569-H I is 40 km/s. Furthermore the age sequence of the super-star clusters is consistent with an interaction scenario as a trigger to the starburst episodes.

It would be illuminating to know at what phase of the interaction the strongest starburst activity is expected to occur. Barnes & Hernquist (1996) state that the timing of an interaction-induced starburst depends on the relative orientations of the two disks and on the pericentric separation at first close approach. Stronger tidal responses in disks are associated with closer passages (or direct collisions) than wider or retrograde encounters. Also the response to a tidal perturbation depends on the internal structure of the galaxy.

8. CONCLUSIONS

We have presented images and spectra of the southern end of the bar in NGC 2366, covering the wavelength range from 115 nm to 2.2 μm. From these data, we deduce the following:

1. The star-forming complex NGC 2366-I and II is a clear example of a multiple-stage starburst, with characteristic ages decreasing from $\sim$ 10 Myr (NGC 2366-II) to $\sim$ 3 - 5 Myr (NGC 2363-B) to $\leq$ 1 Myr (NGC 2363-A).

2. The large number of red supergiants in NGC 2366-II indicates that the bulk of stars formed $\sim$ 10 Myr ago, but the presence of a few bright blue stars close to an intense ridge of ionized hydrogen suggests that star formation went on until more recently ($\sim$ 5 Myr ago).

3. NGC 2363-B contains no red supergiants, but numerous massive O stars, three WR candidates and an erupting LBV, and is located in the middle of an expanding superbubble of dynamical age 3 Myr. The core of cluster B is composed of young (2.5 to 3 Myr) massive stars surrounded by a slightly older (4-5 Myr) population.

4. The kinetic energy released by the winds of massive stars in the core of cluster B (within the FOS aperture) is not sufficient (by a factor of $\sim$ 100) to have blown the expanding superbubble.

5. NGC 2363-A is a very young ($\leq$ 1 Myr) and dense star cluster still embedded in dust. A significant fraction of the UV radiation emitted by its hidden massive stars must leak out of the clumpy dust cloud to provide the bulk of the ionizing flux of the giant H II region.

6. NGC 2366-III is composed of multiple loose OB associations. We suggest that it may be part of a satellite of NGC 2366, whose passage close to the end of the bar some 10 Myr ago initiated the multiple-stage starburst in NGC 2366-II and NGC 2363.

If it were at a distance of 100 Mpc of more, the whole star-forming complex would be less than 1 arcsecond in diameter. The interpretation of its global parameters in terms of multiple starburst episodes would then be hampered by the lack of spatial resolution. Finally, our study of the small starburst NGC 2363 demonstrates vividly how powerful a tool HST has been at helping to unveil the stellar content and evolution of neaby giant star forming regions. The stunning progress in our understanding of giant H II regions can be fully measured by reading the pionneering work on NGC 2363 by Kennicutt *et al.* (1980).

We thank François St-Pierre who did the analysis and derived the parameters of the distant Sc I spiral galaxy seen through the disk of NGC 2366 and Mario Lelièvre who helped with Figure 12. This investigation was funded in part by the Natural Sciences and Engineering Research Council of Canada, by the Fonds FCAR of the Government of Québec and by Université Laval. **Most figures in the astro-ph archives are compressed and dithered. The original figures are available at the following URL: http://astrosun.phy.ulaval.ca/astro/N2363.html**

9. Appendix: Distant Background Galaxies

Table 1 gives the list and coordinates of the background galaxies detected in our WFPC2 V images of the field of NGC 2366, in increasing order of right ascension. Images of these galaxies will be posted on the NED database. The most striking object is the spiral N2366BG7, which has a magnitude V $\sim$ 17.1 and B $-$ V $\approx$ 1.0 (Figure 16). We used this galaxy to derive the reddening through the disk at that location in NGC 2366, and we have estimated its distance. We assumed an intrinsic value for the color of the seen-through spiral first by comparing it to nearby morphological counterparts. We adopted B $-$ V = 0.51, by taking the average color of NGC 628, NGC 5660, NGC 6070 and NGC 6118, fair representatives of Sc I galaxies. Assuming a Galactic extinction of $A_V = 0.13$ along this line of sight (Burstein & Heiles 1984), and an internal extinction due to the inclination of the galaxy of 0.16, the derived extinction due to NGC 2366 is A_V(N2366) $\approx$ 0.35. The K-correction (0.28) was done assuming a redshift of 0.13 based on a distance of $\sim$500 Mpc. The distance was inferred again from a comparison with the apparent diameters of the four sibling galaxies.

REFERENCES

Aller, L. H. 1984, Physics of Thermal Gaseous Nebulae (Dordrecht: D. Reidel)

Barnes, J., & Hernquist, L. 1996, ApJ, 471, 115

Binette, L., Dopita, M. A., & Tuohy, I. R. 1985, ApJ, 297, 476

Blaauw, A. 1991, in The Physics of Star Formation and Early Stellar Evolution, ed. C. J. Lada & N. D. Kylafis (Dordrecht: Kluwer), 125

Braun, R. 1995, A&AS, 114, 409

Burstein, D., & Heiles, C. 1984, ApJS, 54, 33

Charbonnel, C., Meynet, G., Maeder, A., Schaller, G., & Schaerer, D. 1993, A&AS 101, 415

Chini, R., Kreysa, E., Mezger, P. G., & Gemünd, H.-P. 1986a, A&A, 154, L8

Chini, R., Kreysa, E., Mezger, P. G., & Gemünd, H.-P. 1986b, A&A, 157, L1

Churchwell, E. 1991, in The Physics of Star Formation and Early Stellar Evolution, ed. C. J. Lada & N. D. Kylafis (Dordrecht: Kluwer), 221

Churchwell, E., Wolfire, M. G., & Wood, D. O. S. 1990, ApJ, 354, 247

Cox, P., Deharveng, L., & Leene, A. 1990, A&A, 230, 181

Devereux, N. A., & Young, J. S. 1990a, ApJ, 350, L25

Devereux, N. A., & Young, J. S. 1990b, ApJ, 359, 42

Devereux, N. A., & Young, J. S. 1991, ApJ, 371, 515

Devost, D., 1999, AJ, 118, 549

Dionne, D. 1999, M. Sc. thesis, Universit Laval.

Doyon, R., Nadeau, D., Joseph, R. D., Goldader, J. D., Sanders, D. B., & Rowlands, N. 1995, ApJ, 450, 111.

Draine, B. T. 1990, in The Interstellar Medium in Galaxies, ed. H. A. Thronson, Jr. & J. M. Shull (Dordrecht: Kluwer Academic Plublishers), 483

Drissen, L., Moffat, A. F. J., & Shara, M. M. 1993, AJ, 105, 1400

Drissen, L., Roy, J.-R., & Moffat, A. F. J. 1993, AJ, 106, 1460 (DRM)

Drissen, L., Roy, J.-R., & Robert, C. 1997, ApJ, 474, L35-L38

Drissen, L., Crowther, P., Roy, J.-R., Smith, L. J., Hillier, D. J., & Robert, C. 1999a, ApJ, in preparation

Drissen, L., Roy, J.-R., Moffat, A. F. J., & Shara, M. 1999b, AJ, 117, 1249

Eales, S. A., Wynn-williams, C. G., & Duncan, W. D. 1989, ApJ, 339, 859

Garnett, D., Kennicut, R. C., Chu, Y.-H, & Skillman, E. D. 1991, ApJ, 373, 458

Garnett, D. R., Skillman, E. D., Dufour, R. J., Peimbert, M., Torres-Peimbert, S., Terlevich, R., Terlevich, E., & Shields, G. A. 1995, ApJ, 443, 64

González-Delgado, R. M., Perez, E., Tenorio-Tagle, G., Vilchez, J. M., Terlevich, E., Terlevich, R., Telles, E., Rodriguez-Espinosa, J., Mas-Hesse, M., Garcia-Vargas, M. L., Diaz, A. I., Cepa, J., & Castañeda, H. 1994, ApJ, 437, 239

Grevesse, N., Noels, A., & Sauval, A. J. 1996, in Cosmic Abundances, ed. SS. Holt & G. Sonneborn (San Francisco: ASP), 117

Hildebrand, R. H. 1983, QJRAS, 24, 267

Hildebrand, R. H., Whitcomb, S. E., Winston, R., Stiening, R. F., Harper, D. A., & Moseley, S. H. 1977, ApJ, 216 698

Hollenbach, D., Johnstone, D., Lizano, S., & Shu, F. 1994, ApJ, 428, 654

Hunter, D. A., & Gallagher, J. S. 1997, ApJ, 475, 65

Izotov, Y. I., Thuan, T. X., & Lipovetsky, V. A. 1997, ApJS, 108, 1

Kennicutt, R. C. 1983, ApJ. 272, 54

Kennicutt, R. C. 1984, ApJ, 287, 116

Kennicutt, R. C., Balick, B., & Heckman, T. 1980, PASP, 92, 134

Keyes, C. D., Koratkar, A. P., Dahlem, M., Hayes, J., Christensen, J. & Martin, S. 1995, Faint Object Spectrograph Instrument Handbook, version 6.0.

Kurucz, R.L. 1992, in IAU Symp. 149, *The Stellar Population of Galaxies*, ed B. Barbuy, & A. Renzini (Dordrecht: Kluwer), 225

Leitherer, C., Robert, C., & Drissen, L. 1992, ApJ, 401, 596

Leitherer, C., Schaerer, D., Goldader, J. D., Gonzlez-Delgado, R., Robert, C., Foo Kune, D., de Mello, D. F., Devost, D., & Heckman, T. M. 1999, ApJS, 123, 3

Luridiana, V. 1998, in Abundance Profiles: Tools for Galaxy History, ASP Conf. Ser. 147, ed. D. Friedli, M. Edmunds, C. Robert & L. Drissen, (San Francisco), p. 138

Maeder, A. 1999, A&A, 347, 185

Maeder, A., & Meynet, G. 1987, A&A, 182, 243

Martin, C. 1998, ApJ, 506, 222

Mayya, Y. D. 1997, ApJ, 482, L149

Meynet, G., Maeder, A., Schaller, G., Schaerer, D., & Charbonnel, C. 1993, A&AS 103, 97

Nadeau, D., Murphy, D. C., Doyon, R., & Rowlands, N. 1994, PASP, 106, 909

Osterbrock, D. E. 1989, Astrophysics of Gaseous Nebulae and Active Galactic Nuclei (Mill Valley: University Science Books), 210

Pakull, M. M., & Angebault, L. P. 1986, Nature, 322, 511

Pakull, M. M. 1991, in IAU Symp. 143, Wolf-Rayet Stars and Their Interrelations with Other Massive Stars in Galaxies, ed. K. van der Hucht & B. Hidayat (Dordrecht: Kluwer), 260

Peimbert, M., Peña, M., & Torres-Peimbert, S. 1986, A&A, 158, 266

Prevot, M. L., Lequeux, J., Prevot, L., Maurice, E., Rocca-Volmerange, B. 1984, A&A 132, 389

Roy, J.-R., Boulesteix, J., Joncas, G., & Grundseth, B. 1991, ApJ, 367, 141

Roy, J.-R., Aubé, M., McCall, M. L., & Dufour, R. J. 1992, ApJ, 386, 498

Roy, J.-R., Belley, J., Dutil, Y., & Martin, P. 1996, ApJ, 460, 284

Sauvage, M., & Thuan, T. X. 1992, ApJ, 396, L69

Schaerer, D., Meynet, G., Maeder, A., & Schaller, G. 1993a, A&AS 98, 523

Schaerer, D., Charbonnel, C., Meynet, G., Maeder, A., & Schaller, G. 1993b, A&AS 102, 339

Schaerer, D., & Vacca, W. D. 1998, ApJ, 497, 618

Schaller, G., Schaerer, D., Meynet, G., & Maeder, A. 1992, A&AS 96, 269

Schmutz, W., Leitherer, C., Gruenwald, R. 1992, PASP 104, 1164

Silva, L., Granato, G. L., Bressan, A., & Danese, L. 1998, ApJ, 509, 103

Solomon, P. M., Downes, D., Radford, S. J. E., & Barrett, J. W. 1997, ApJ, 478, 144

Stil, J. M., & Israel, F. P. 1998, A&A, 337, 64

Sutherland, R. S., Bicknell, G. V., & Dopita, M. A. 1993, ApJ, 414, 510

Taylor, C. L. 1995, Ph. D. Thesis, University of Minnesota

Taylor, C. L. Brinks, E., Grashuis, R. M., & Skillman, E. D. 1995, ApJS, 99, 427

Tolstoy, E., 1995, Ph. D. Thesis, Rijksuniversiteit Groningen

Tolstoy, E., Saha, A., Hoessel, J. G., & McQuade, K. 1995, AJ, 110, 1640

Walborn, N. R., Nichols-Bohlin, J., & Panek, R.J. 1985, NASA Ref. Pub. 1155

Whitmore, B. 1995, in Calibrating Hubble Space Telescope: Post Servicing Mission, ed. A. Koratkar & C. Leitherer (Baltimore: Space Telescope Science Institute), 269

Wood, D. O. S., & Churchwell, E. 1989a, ApJ, 340, 265

Wood, D. O. S., & Churchwell, E. 1989b, ApJS, 69, 831

Table 1. Background Galaxies in the field of NGC 2366

Object	α (2000)	δ (2000)	V	Comment
N2366BG1	07 28 38.7	69 12 19.2	23.4	
N2366BG2	07 28 39.0	69 11 47.3	23.4	
N2366BG3	07 28 43.0	69 12 02.2	21.2	
N2366BG4	07 28 43.2	69 12 39.3	21.9	
N2366BG5	07 28 43.2	69 12 46.1	23.0	
N2366BG6	07 28 44.2	69 12 05.0	23.1	
N2366BG7	07 28 45.3	69 12 19.2	17.1	Scd (see Figure 16)
N2366BG8	07 28 45.9	69 12 40.9	22.6	
N2366BG9	07 28 47.9	69 12 40.0	21.4	
N2366BG10	07 28 51.1	69 11 21.1	21.6	
N2366BG11	07 28 51.3	69 12 02.9	21.3	
N2366BG12	07 28 53.3	69 11 21.0	21.9	
N2366BG13	07 28 54.5	69 11 12.0	19.3	Interacting with N2366BG14?
N2366BG14	07 28 54.6	69 11 11.3	21.1	Interacting with N2366BG13?

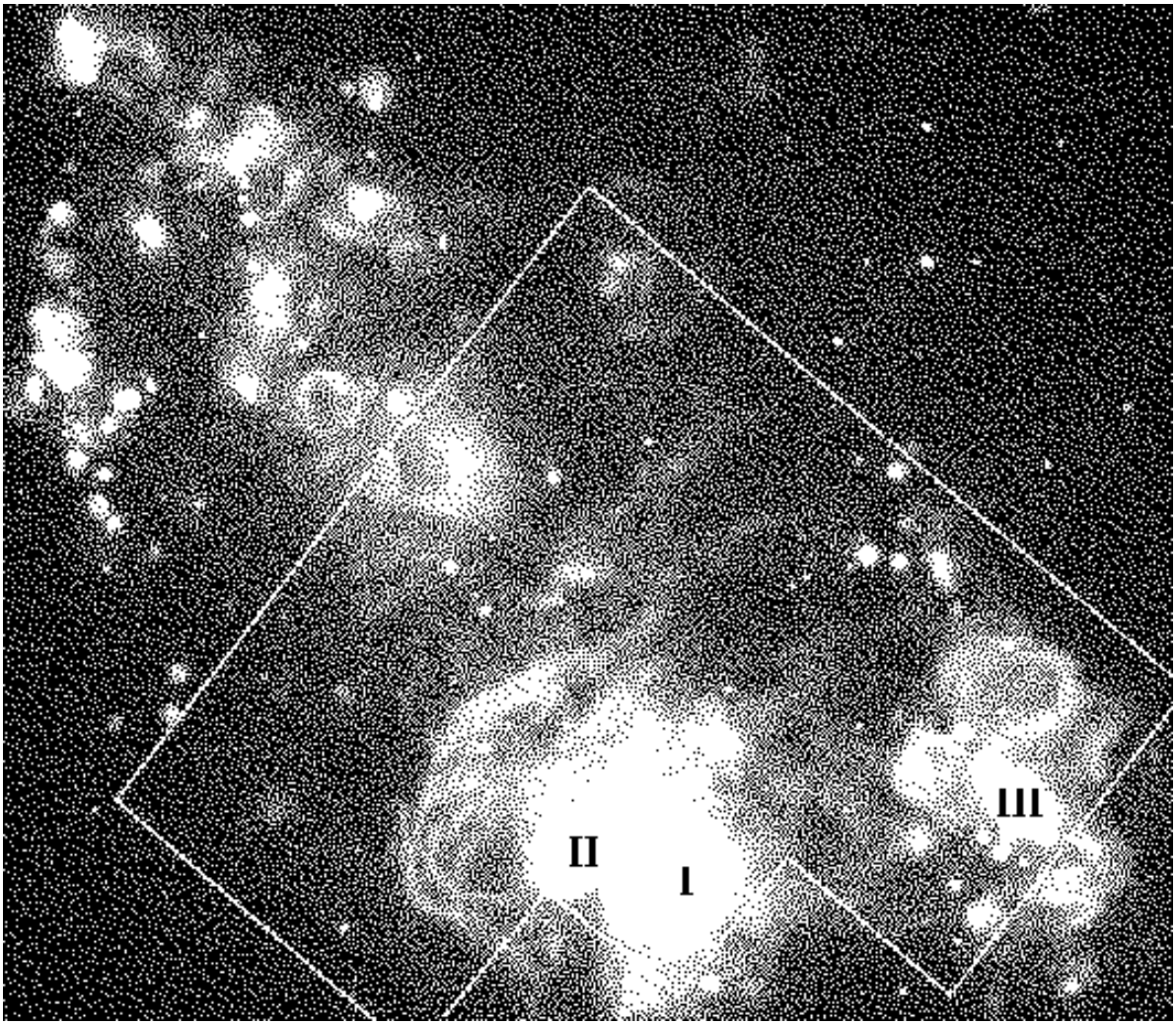

Fig. 1.— Hα image of NGC 2366 from the CFHT. The HST/WFPC2 field of view is outlined, and the giant H II regions are numbered. The field is $230'' \times 195''$ (3.8 kpc $\times$ 3.2 kpc at the distance of NGC 2366). North is up, east to the left.

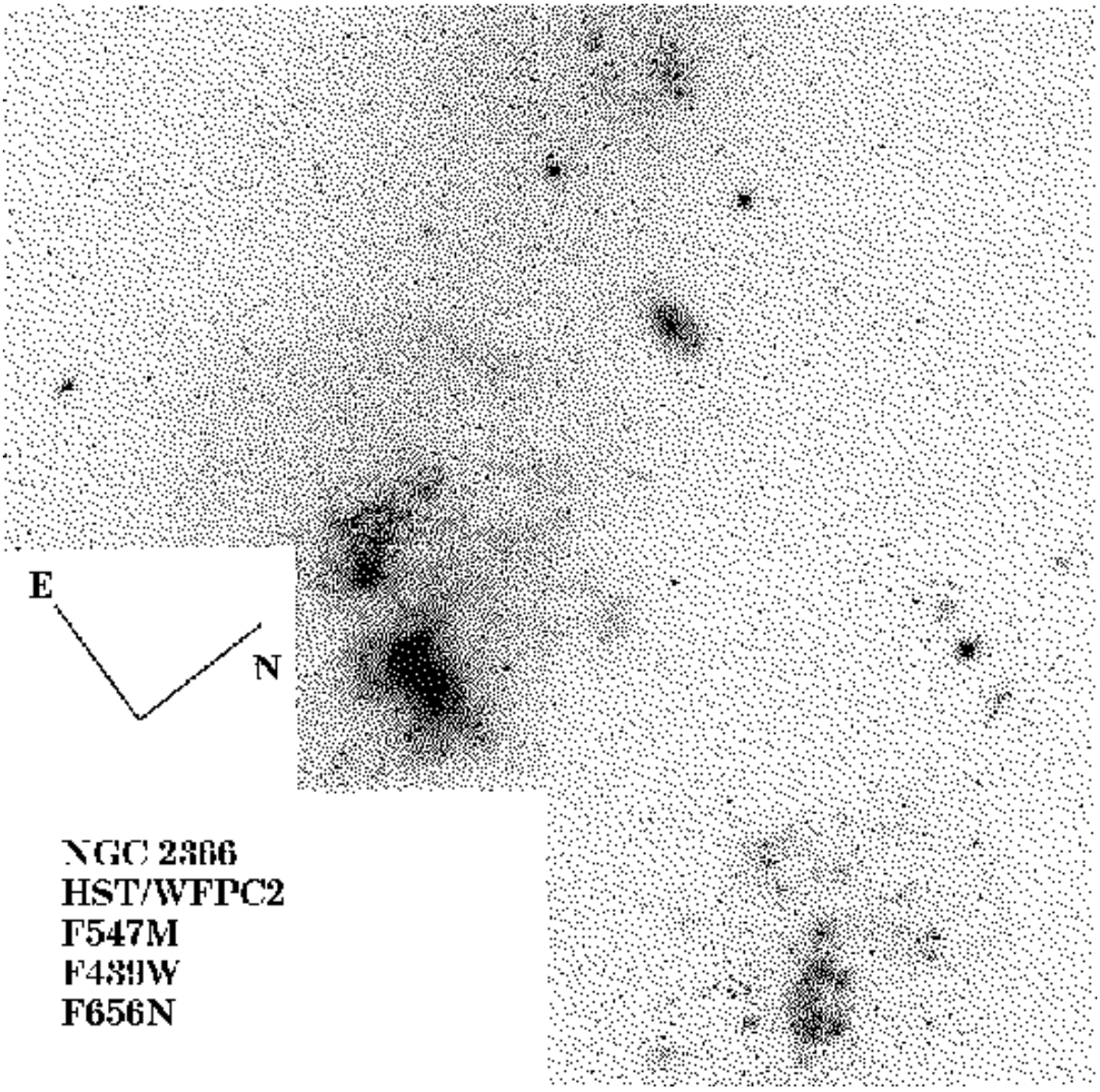

Fig. 2.— Color-composite WFPC2 image of NGC 2366. Full resolution color image available at http://astrosun.phy.ulaval.ca/astro/N2363.html

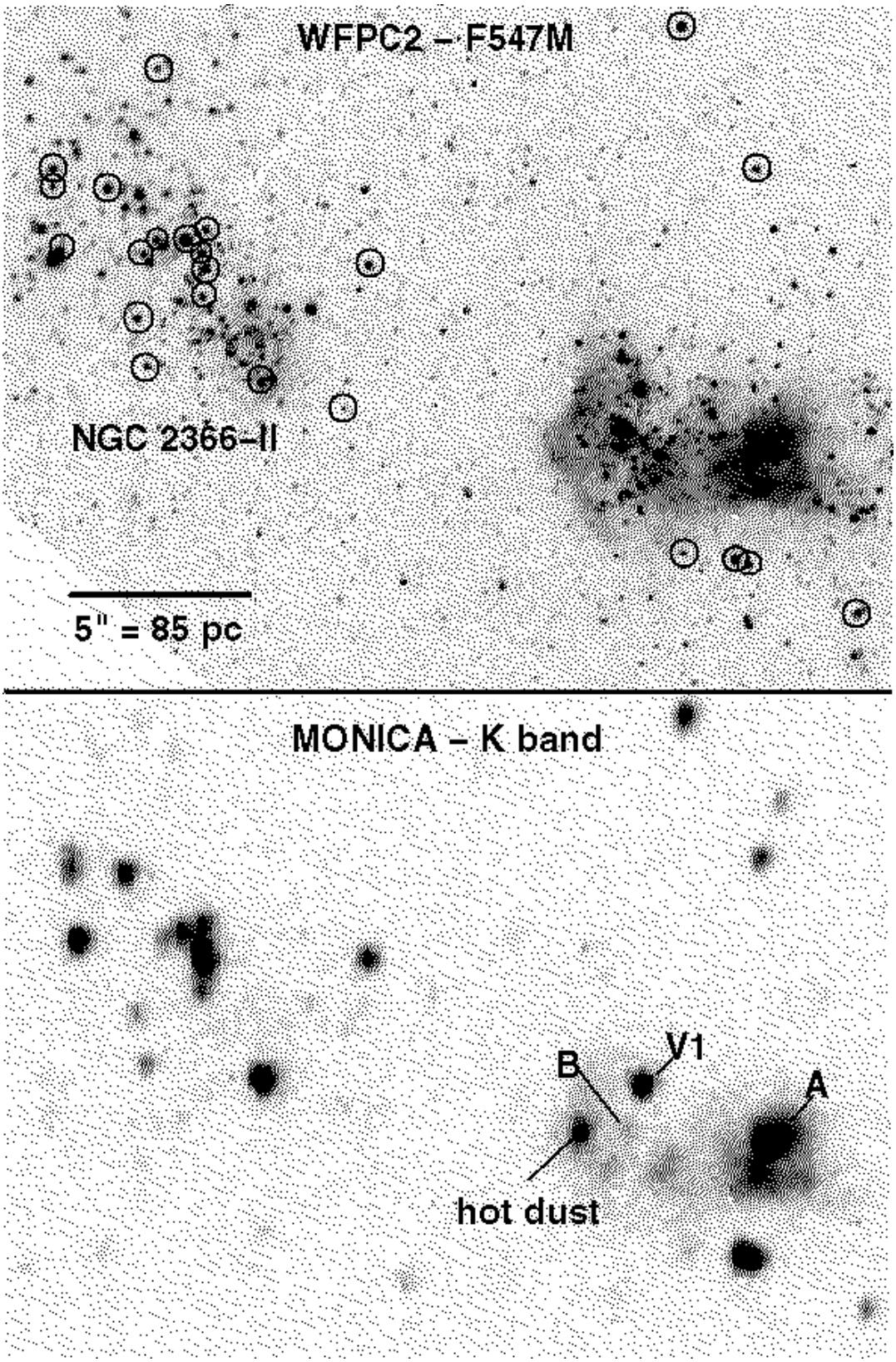

Fig. 3.— HST/WFPC2 and CFHT/Monica images of NGC 2363(right) and NGC 2366-II (left). The red supergiant stars identified in the color-magnitude diagram (in Figure 4, with $B - V \geq 1.0$ and $M_V \leq -5.0$) are circled on the WFPC2 image; these are prominent in the K-band image. Note that cluster A is very bright in K, contrary to cluster B, as well as the possible presence of hot dust (see text).

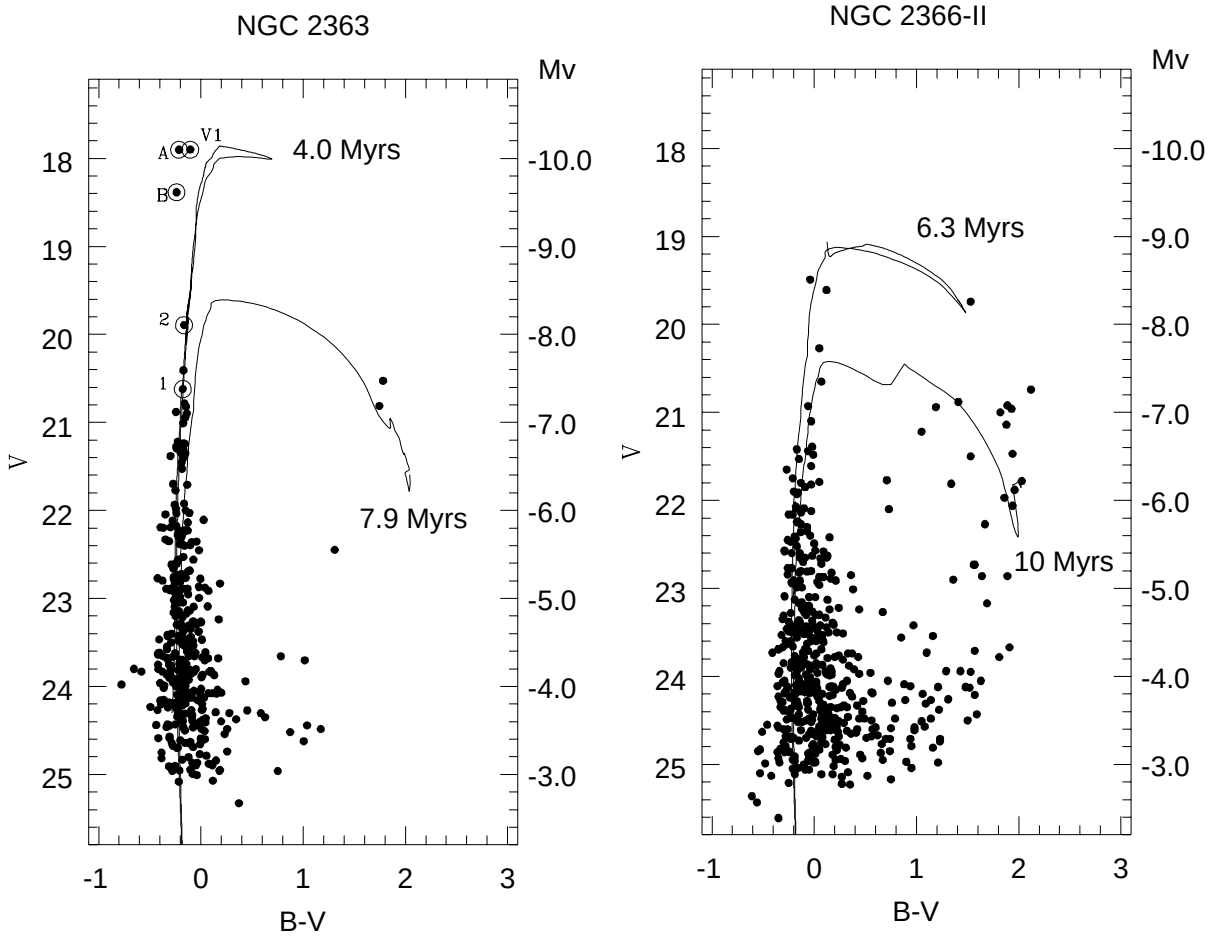

Fig. 4.— Color-Magnitude diagram of NGC 2363 and NGC 2366-II. The magnitudes of clusters A and B in NGC 2363 are measured with an aperture of r = 0.43″ to match that of the FOS spectrograms.

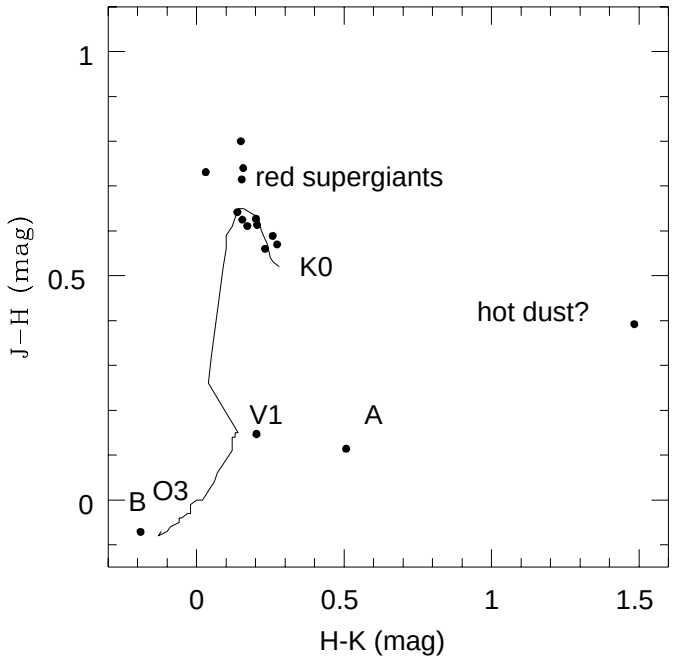

Fig. 5.— Near-infrared two-color diagram of NGC 2363 and NGC 2366-II. The location of the supergiant sequence (from O3 to K0) is shown for comparison. Knots A and B, as well as NGC 2363-V1 and the hot dust patch are identified.

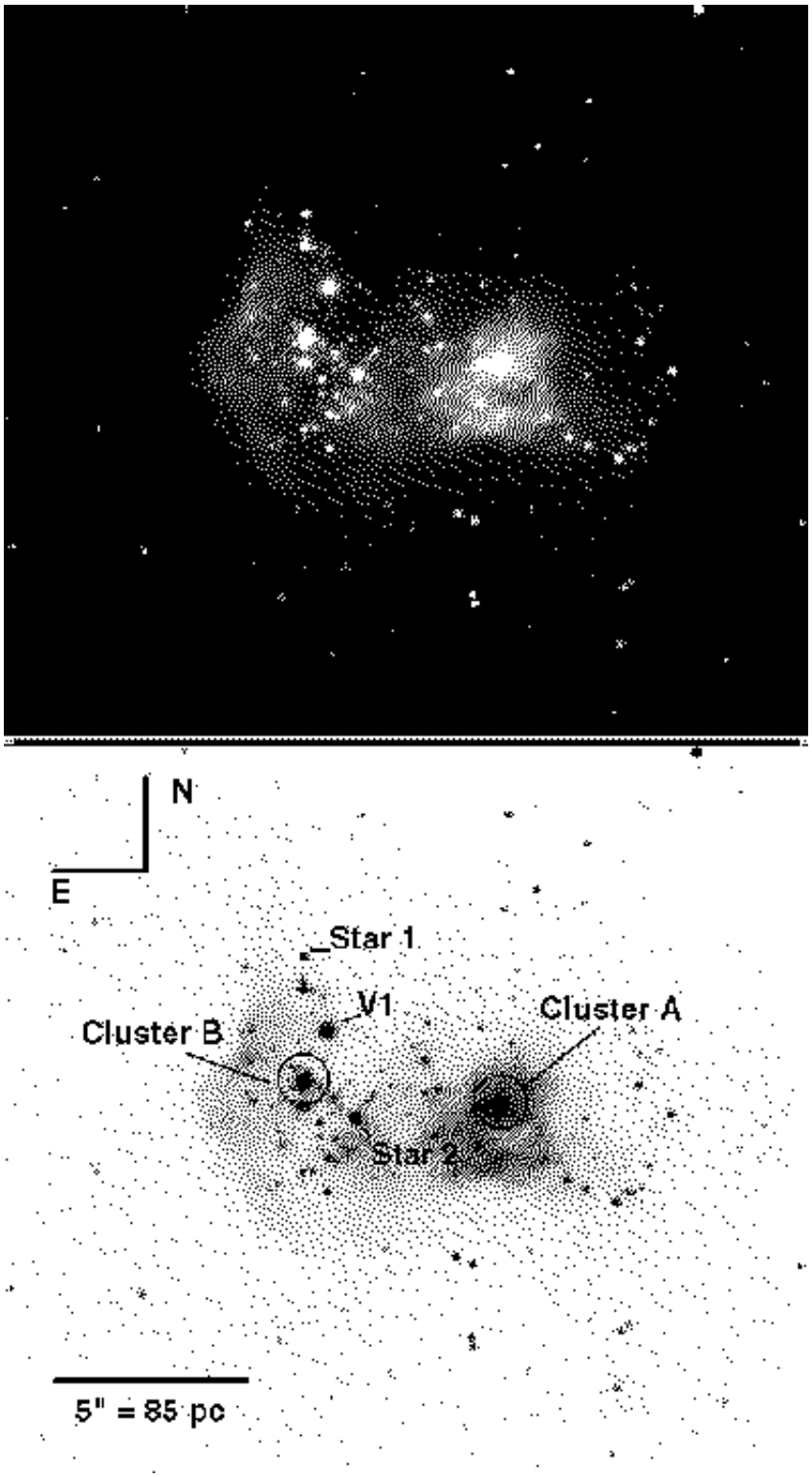

Fig. 6.— [top] Color-composite WFPC2 image of NGC 2363 with the B (F439W) frame in the blue beam, the average of the B and V (F547M) frames in the green beam and the average of the V and $H\alpha$ (F656N) frames in the red beam. The field of view is $21'' \times 19''$ (350×325 pc). [bottom] Same image as above showing the different objects described in the text; the two HST/FOS apertures are also shown as circles.

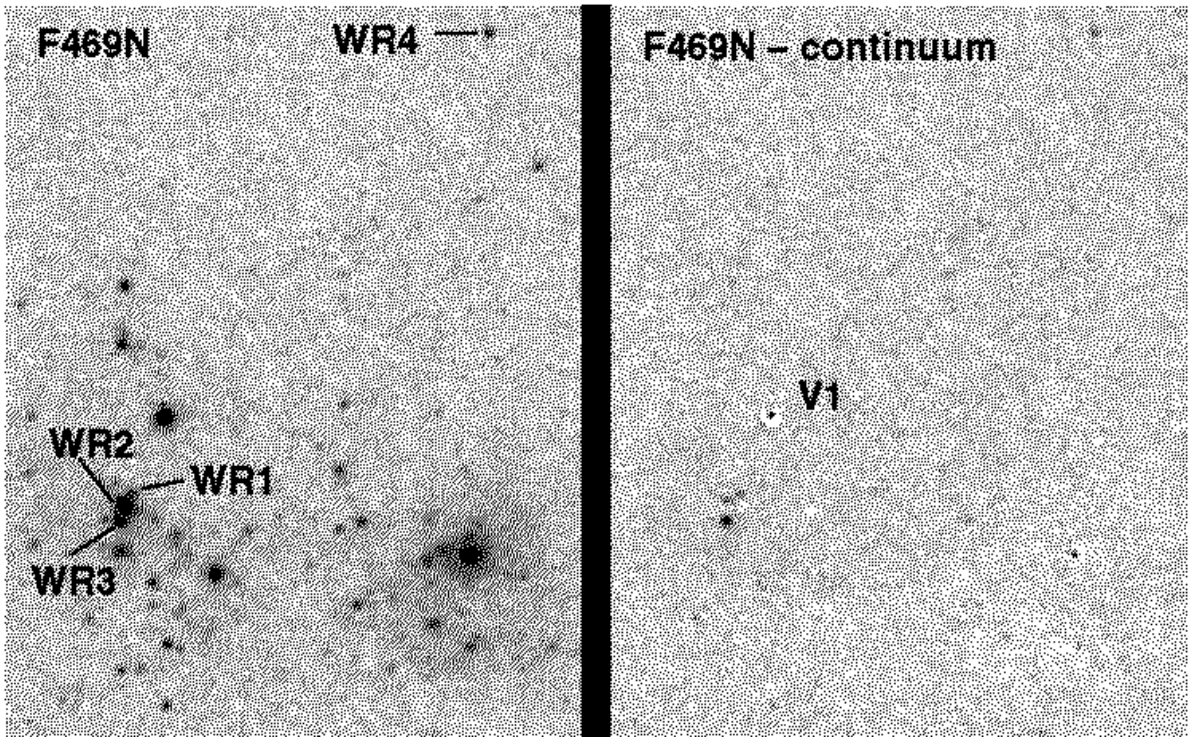

Fig. 7.— F469N (He II λ4686) and net 4686 images of NGC 2363. WR candidates are identified. Note the positive and negative pixels at the location of V1 and cluster A; these artefacts are the result of the imperfect image subtraction and show up because the two objects are by far the brightest in the image, but they do not represent significant He II enhancements. http://astrosun.phy.ulaval.ca/astro/N2363.html

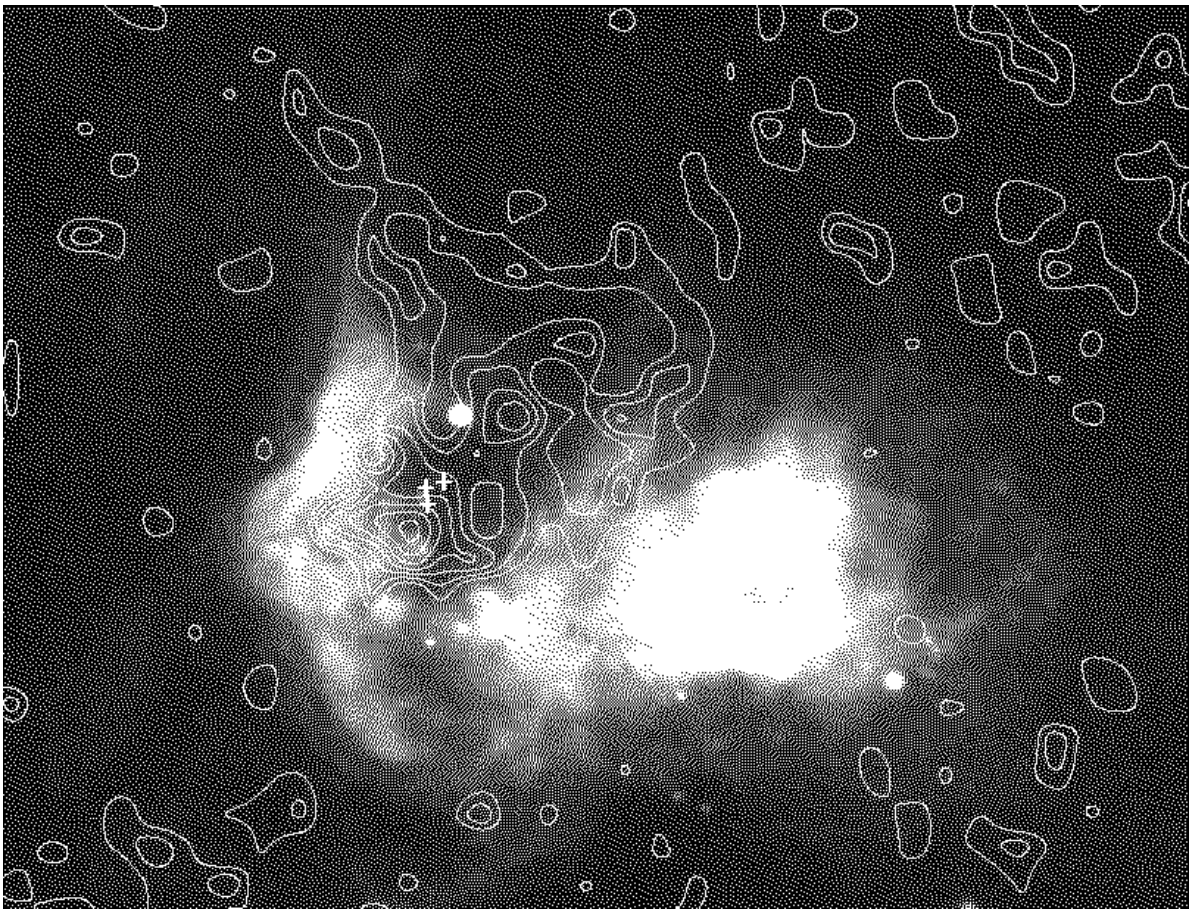

Fig. 8.— Hα image of NGC 2363, with contours of the He II 4686 diffuse excess. The point sources identified as Wolf-Rayet stars have been removed from the net λ 4686 image and marked here as plus signs. The lowest contour corresponds to 0.5σ (standard deviation from the sky background), with increments of 0.5σ per contour level up to 0.35σ. Note the spatial correspondance with the apparent Hα cavity.

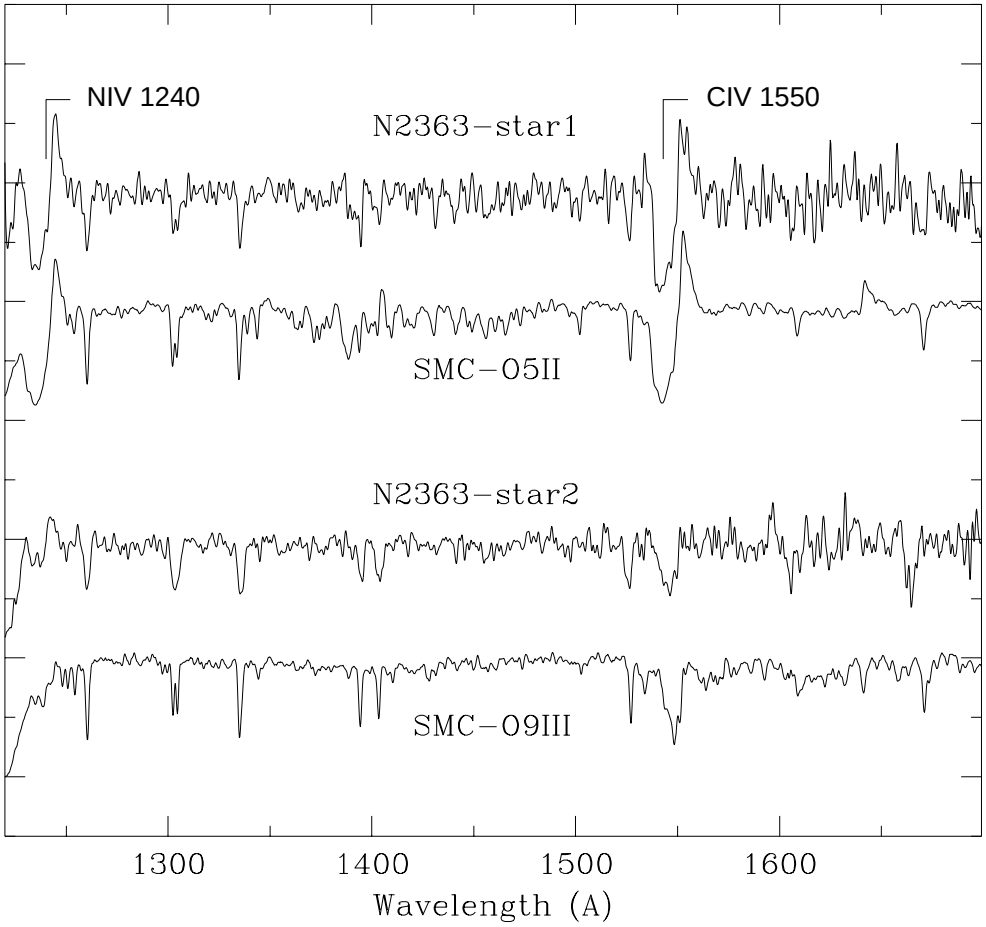

Fig. 9.— STIS spectra of stars 1 and 2 (identified in Figure 6). For comparison, representative spectra of stars with similar spectral characteristics in the SMC are also shown.

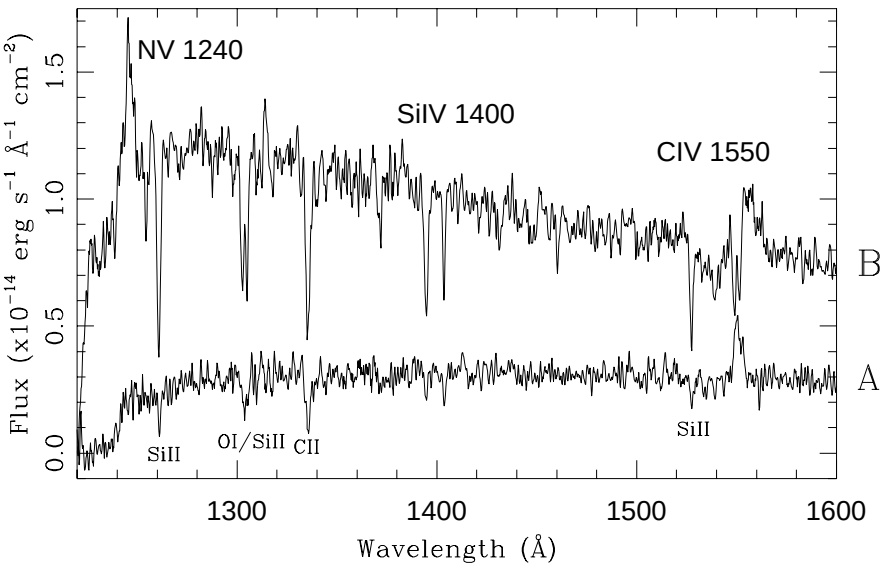

Fig. 10.— Flux-calibrated HST/FOS spectra of knots A and B.

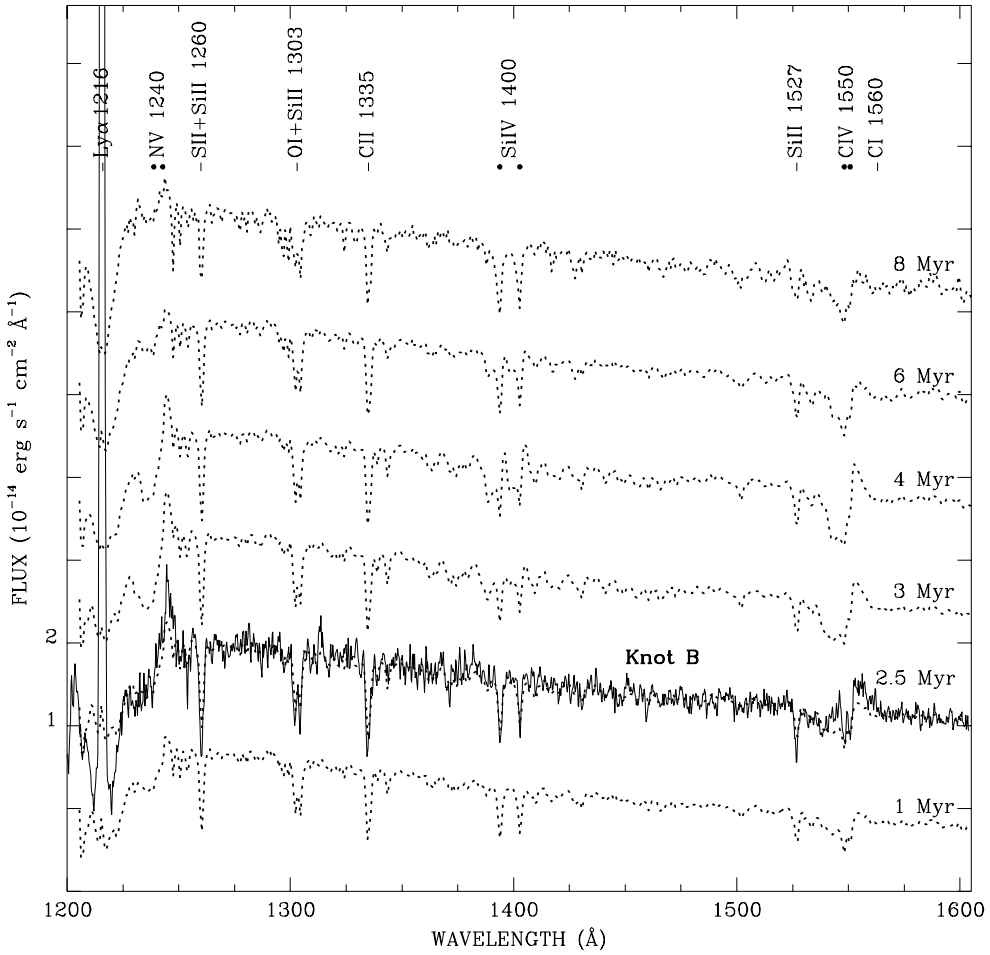

Fig. 11.— Comparison of synthetic UV spectra for knot B. The spectra of knot B (full line) is dereddened using $E(B-V) = 0.058$ and an SMC reddening law. Synthetic spectra (dotted lines) for various ages have been calculated for an instantaneous burst using the stellar evolutionary tracks at a metallicity 0.1 $Z_{\odot}$, the SMC spectral library, and a Salpeter type IMF ($\alpha = 2.35$) with stars between 1 and 80 $M_{\odot}$. All the synthetic spectra, except the one at 2.5 Myr, are shifted. The strongest interstellar and stellar lines are identified at the top. A dot preceding the line identification indicates a line formed mainly in hot star winds. The synthetic spectrum at 2.5 Myr is the best model retained based on the UV line synthesis.

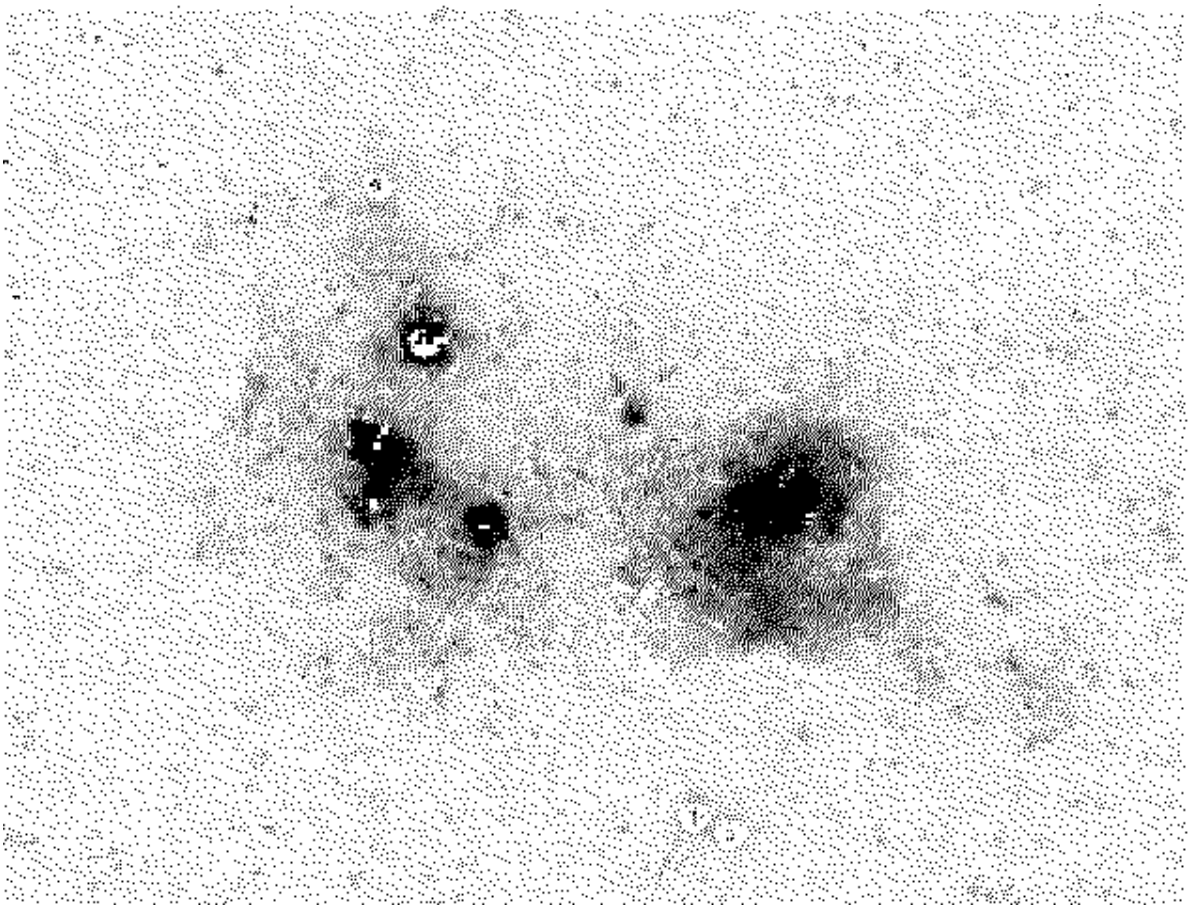

Fig. 12.— Diffuse stellar light in the F547M WFPC2 filter scattered by interstellar dust in NGC 2363. Display is in logarithmic scale.

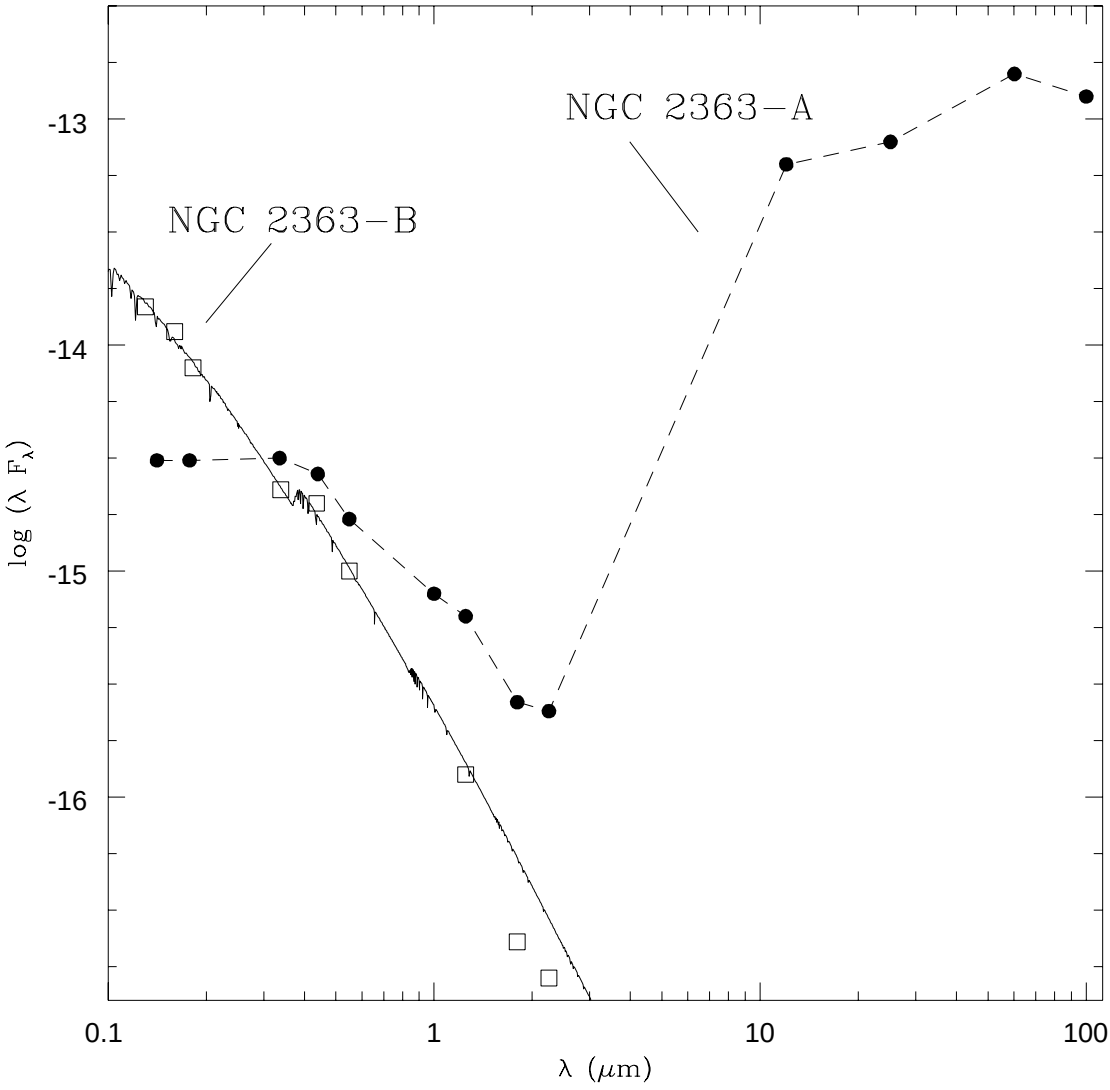

Fig. 13.— Spectral energy distribution of NGC 2363-A and B. The solid line joining the data points for NGC 2363-B is the energy distribution of an instantaneous starburst aged 3 Myrs. The dotted line joining the data points for NGC 2363-A is just intended to guide the eye; no attempt to fit a model distribution was made.

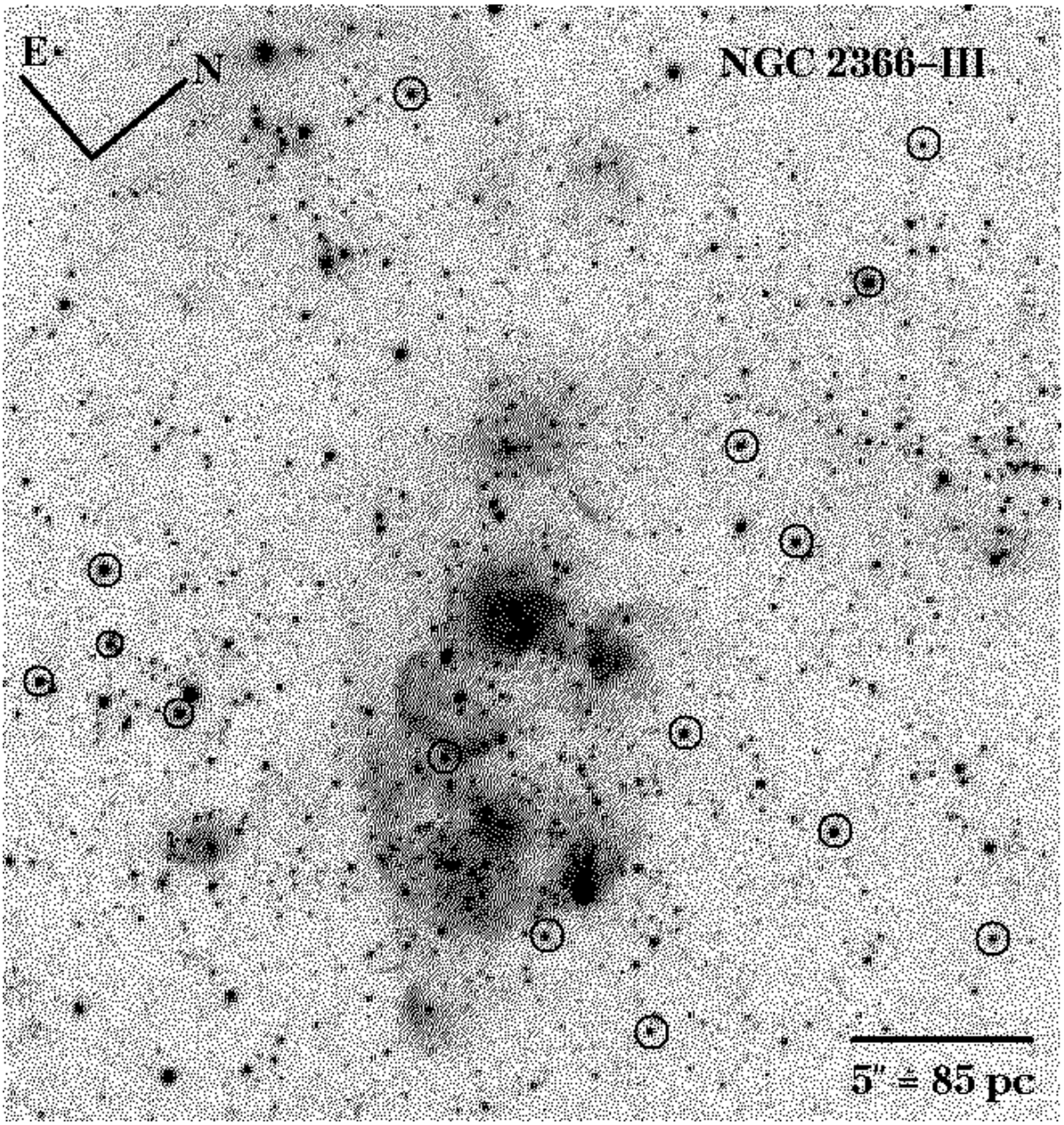

Fig. 14.— WFPC2 image of the central region of NGC 2366-III. Red supergiant stars are marked.

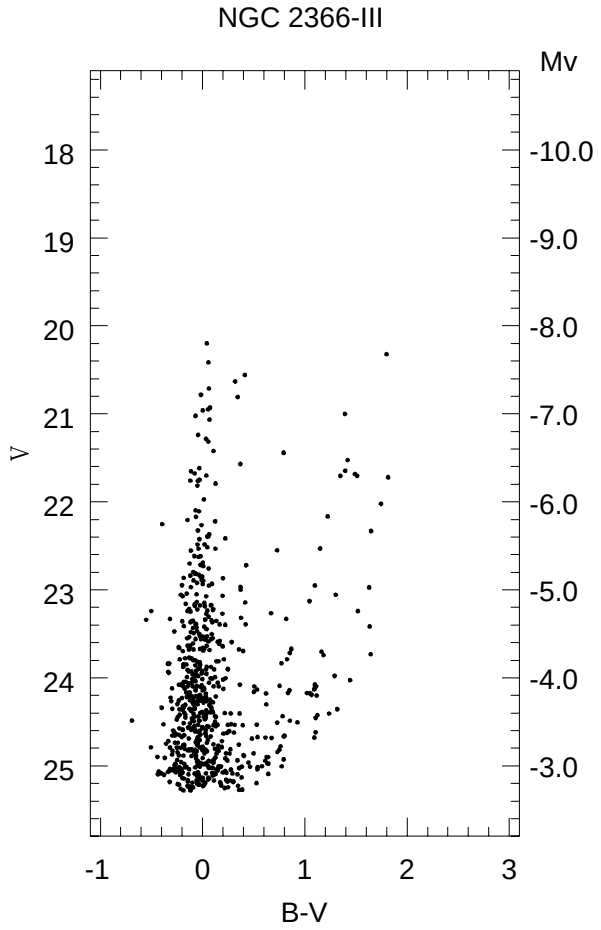

Fig. 15.— Color-magnitude diagram of NGC 2366-III.

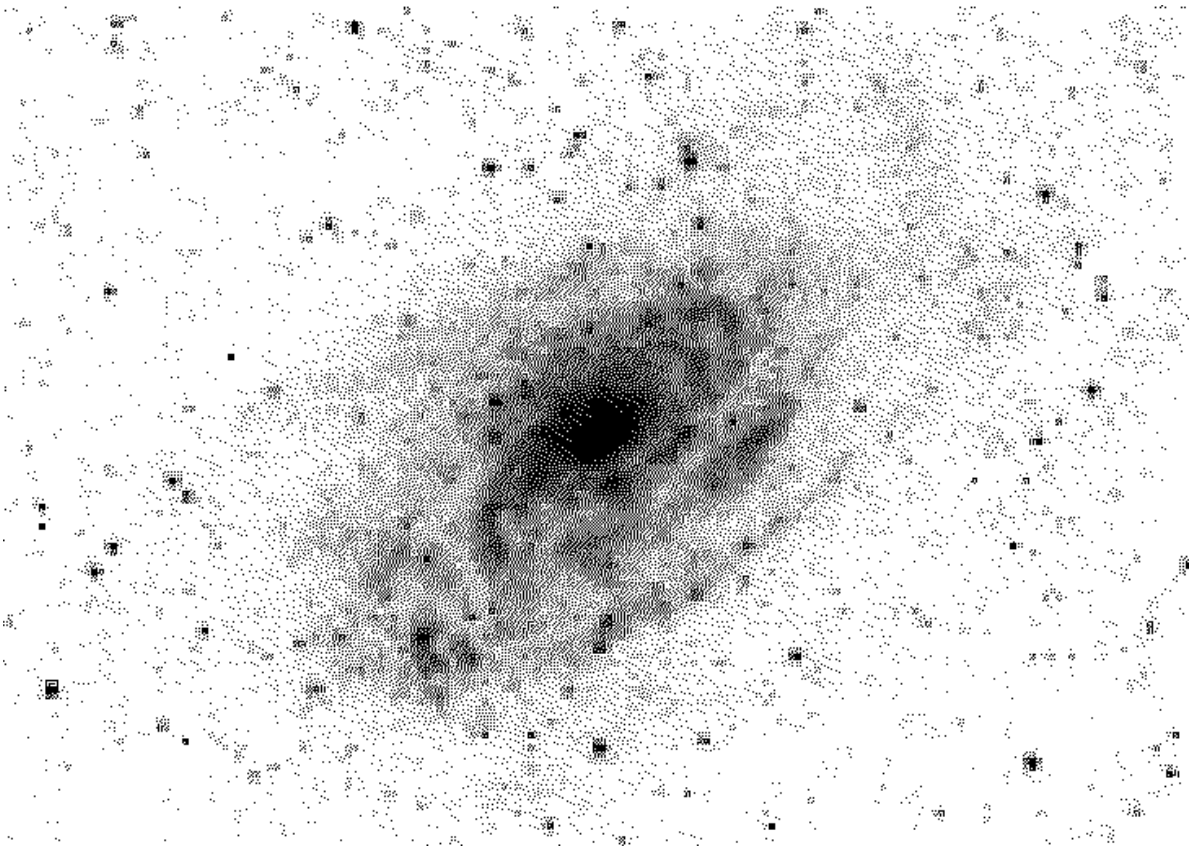

Fig. 16.— Distant Sc spiral galaxy at $d \sim 500$ Mpc seen through the disk of NGC 2366. The scale of the image is 18×13 arcsec^2.